Dissertation
submitted to the
Combined Faculties for the Natural Sciences and for Mathematics
of the Ruperto-Carola University of Heidelberg, Germany
for the degree of
Doctor of Natural Sciences

presented by:

Dipl.-biol. Mercedes Laura Dragovits
born in: Buenos Aires, Argentina
Oral examination: 13th January 2012

Regulation of Cell Adhesion and Fibronectin Fibrillogenesis by Biomimetic Substrates

Referees:

PD Dr. Suat Özbek
Prof. Dr. Joachim P. Spatz

Contents

1 Summary

Integrins are transmembrane receptors which modulate a wide variety of cellular functions, like survival, proliferation, adhesion and extracellular matrix (ECM) assembly. The major ligand of $\alpha_5\beta_1$-integrin is fibronectin (FN), a key component of the ECM. This glycoprotein can be found as fibrillar network in different tissues (cellular FN, cFN) or circulating in plasma (plasma FN, pFN). These two physiologically ocurring types of FN also differ in their structure and composition due to alternative splicing.

The objective of this work was to analyze how the different FNs affect cell spreading and the formation of adhesion sites. Therefore, glass substrates were coated with either pFN or cFN and cell responses were monitored by phase contrast or fluorescence microscopy. Cell spreading kinetics was similar on both substrates. However, it was observed for the first time that there were differences in the distribution and shape of adhesion sites; while different focal adhesion (FA) markers localized over the whole cell area on cFN, they were found preferentially at the cell periphery on pFN coatings. In addition, cFN favoured a more elongated shape of adhesion sites, a faster translocation of $\alpha_5\beta_1$-integrin and FN fibril formation, showing that the molecular composition of this protein affects in turn FN assembly.

Fibroblasts were seeded on gold nanopatterned surfaces biofunctionalized with cyclic RGD peptides targeting mainly $\alpha_v\beta_3$-integrin. On substrates presenting an interligand distance of 58 nm, fibroblasts formed actin stress fibers and FN fibrils. In contrast, FN was only detected as dot-shaped accumulations on samples with a higher interligand distance (73 nm or 110 nm), indicating that 58 nm is a critical interligand distance for $\alpha_v\beta_3$-integrin that promotes both the formation of stress fibers and FN assembly.

In this study I could show that distinct FNs and the spatial organization of integrin ligands differentially affect cell adhesion and FN deposition. In addition, these results reinforce the correlation between FA and fibrillar adhesion formation, indicating that FN assembly can be regulated by controlling cell adhesion through substrate functionalization.

2 Zusammenfassung

Integrine sind Transmembranrezeptoren, welche ein breites Spektrum unterschiedlicher Zellfunktionen, wie das Überleben, die Proliferation, die Adhäsion und die Bildung der extrazellulären Matrix (ECM) regulieren. Der wichtigste Ligand des $\alpha_5\beta_1$-Integrins ist das Fibronektin (FN), eine Hauptkomponente der ECM. Dieses Glykoprotein kommt in diversen Geweben als fibrilläres Netzwerk (zelluläres FN, cFN) oder im Plasma (Plasma FN, pFN) vor. Diese zwei physiologisch vorkommenden FN-Typen unterscheiden sich aufgrund von alternativem Spleißen auch in ihrer molekularen Zusammensetzung und Struktur.
Das Ziel dieser Arbeit war, die Einflüsse beider FNs sowohl auf die Zellausbreitung als auch auf die Bildung von Adhäsionsstellen zu analysieren. Die Zellausbreitung war auf beiden Substraten ähnlich. Zum ersten Mal wurden allerdings Unterschiede in der Verteilung und Form von Adhäsionsstellen aufgezeigt. Fokaladhäsionen (FA) wurden auf der gesamten Zellfläche auf cFN , während sie auf pFN vorzugsweise in der Zellperipherie beobachtet wurden. Darüber hinaus wurde gezeigt, dass cFN eine länglichere Form von Adhäsionsstellen, eine schnellere Translokation von $\alpha_5\beta_1$-Integrin sowie FN Fibrillenbildung förderte.
Fibroblasten wurden auf Gold-Nanostrukturen, welche mit $\alpha_v\beta_3$-Liganden funktionalisiert wurden, gesetzt. Aktin Stressfasern und FN Fibrillen wurden auf Substraten beobachtet, die einen Interliganden-Abstand von 58 nm aufwiesen, im Gegensatz zu Proben mit einem größeren Abstand, auf denen FN lediglich als punktförmige Aggregate sichtbar war. Diese Ergebnisse zeigten, dass 58 nm ein kritischer Abstand von $\alpha_v\beta_3$-Liganden ist, welcher die Bildung von Stressfasern und FN-Fibrillen begünstigte.
In dieser Studie konnte ich zeigen, dass die molekulare Zusammensetzung von FN und die räumliche Anordnung von Integrinliganden einen Einfluss auf die Zelladhäsion und die Ablagerung von FN haben. Diese Ergebnisse unterstreichen den Zusammenhang zwischen der Bildung von FA und fibrillären Adhäsionen. Darüber hinaus wurde gezeigt, dass die Assemblierung von FN durch die Regulierung von Zelladhäsion mittels Substratfunktionalisierung beeinflusst werden kann.

3 Introduction

Multicellular organisms are composed of cells assembled into tissues and cells that circulate in the bloodstream. Tissue cells contact and interact with neighbouring cells and with the acellular material they produce and locally deposit - referred to as extracellular matrix (ECM).
The most common cell type in connective tissues are fibroblasts, which secrete and assemble proteins of the ECM and are involved in angiogenesis. Therefore, they play an important role in wound healing [Werner et al., 2007] as well as in cancer progression [Kalluri and Zeisberg, 2006].
One of the main cell adhesive components of the ECM is fibronectin, a glycoprotein that can be found in connective tissues and circulating in the bloodstream. It is indispensable during development [George et al., 1993] and is involved in pathologies, including different types of cancer and fibrosis [Allen and Jones, 2011]. Although the molecular mechanisms underlying its functions have been extensively studied, they still remain largely unknown.
This study focusses on the mechanism underlying fibroblast adhesion to fibronectin and its assembly into a fibrillar network.

3.1 Cell adhesion

Cell adhesion can be grouped in two categories: cell-cell and cell-matrix adhesion. Cell-cell interactions are regulated by multiple cell adhesion molecules (CAMs), which include cadherins, Ig-superfamily CAMs, selectins, mucins and integrins [Lodish et al., 2000]. Cell-matrix adhesion is modulated mainly by heterodimeric integrins, which bind fibronectin, laminin, collagen, and other matrix proteins. Together, these interactions allow cells to adhere to each other, interconnect the cytoskeletons of adjacent cells, and give tissues their strength and resistance to shear forces.
The types of molecules involved in cell adhesion are represented schematically in figure 3.1.

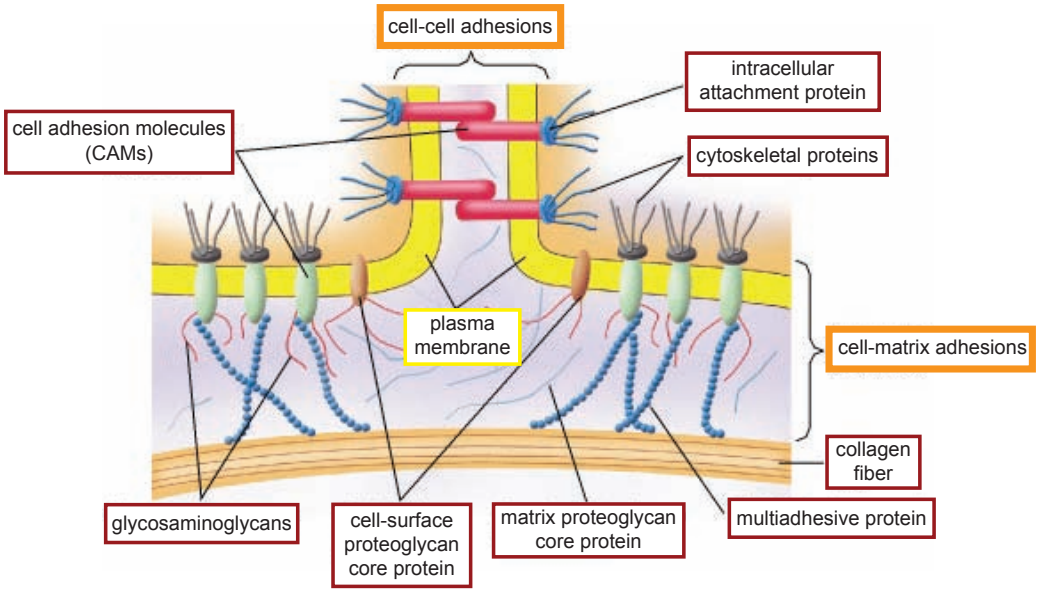

Figure 3.1: **Schematic overview of the types of molecules that regulate cell-cell and cell-matrix adhesion.** Cell-adhesion molecules (CAMs) connect cytoskeletal proteins with similar molecules on other cells or with components of the extracellular matrix. Multiadhesive proteins and proteoglycans bind to cell-surface receptors and to other matrix components. (Adapted from Lodish et al., 2002)

A dysfunction in cell adhesion can lead to pathological conditions, including cancer invasion and metastasis or immune disorders [Guadamillas et al., 2011].

3.1.1 Integrin-mediated cell adhesion

Cell adhesion to the ECM is modulated by interactions between plasma membrane and matrix-associated molecules. The major membrane receptors involved in these interactions belong to the integrin family.
The formation of cell-matrix adhesions is a dynamic and temporally regulated process [Geiger and Yamada, 2011]. An overview of the components of cell-matrix adhesions is shown in figure 3.2 [Zaidel-Bar et al., 2004].
In some cells, such as chondrocytes, one of the first steps in surface recognition is mediated by a hyaluronan pericellular coat [Zimmerman et al., 2002]. After attachment, focal complexes (FX) are formed at the edge of lamel-

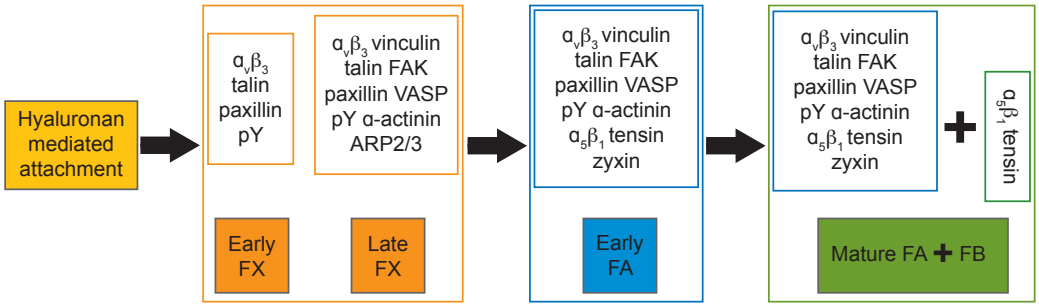

Figure 3.2: **Evolution of adhesion sites** The scheme depicts the molecular composition of the different cell-matrix adhesions, starting with hyaluronan-mediated attachment to focal complexes (FX), focal adhesions (FA) and fibrillar adhesions (FB). (Adapted from Zaidel-Bar, 2004)

lipodia. FXs have a typical area of approx. 0.25 μm^2 and persist for a few minutes. Early FXs contain $\alpha_v\beta_3$-integrins, talin, phosphotyrosine and paxillin. Further proteins are recruited to these structures to give rise to focal adhesions (FA), which link the ECM to the cytoskeleton through intracellular anchor proteins, such as zyxin and tensin. The recruitment of some proteins to FAs is force-dependent. For example vinculin, a protein that connects integrins to actin filaments [Bershadsky et al., 2003], is found under low force in disassembling or sliding FAs at the trailing edge of migrating cells. Mediated by interactions with talin, vinculin induces FA growth [Humphries et al., 2007].
As force is applied to FAs, tensin and $\alpha_5\beta_1$-integrins translocate centripetally

at a rate of 6.5 ± 0.7 μm/h [Pankov et al., 2000] resulting in the formation of fibrillar adhesions (FBs) and ECM remodeling. The formation of FBs was shown to depend on actomyosin contractility and matrix reorganization [Zamir et al., 2000].

3.1.2 The integrin superfamily

The main plasma membrane receptors mediating cell adhesion to extracellular matrix (ECM) ligands belong to the superfamily of non-covalently linked heterodimeric integrins [Humphries et al., 2006]. At least 24 different members result from the combination of type I transmembrane α and β subunits [Hynes, 2002]. The different subunits are shown in figure 3.3.

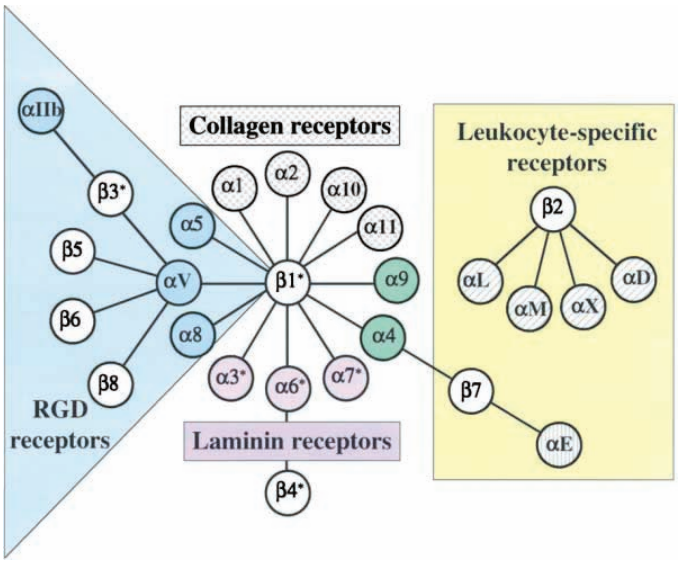

Figure 3.3: **The integrin superfamily.** Integrins are dimeric proteins consisting of α and β subunits. At least 24 different integrins result from the combination of these monomers (Figure from Hynes, 2002)

Integrins not only regulate cell-adhesion and ECM assembly [Hynes, 2002], but are also crucial in embryonic development, angiogenesis, tissue repair and hemostasis [Harburger and Calderwood, 2009]. Furthermore, they are important for hematopoiesis, leukocyte trafficking and formation of immunological synapses, making integrin-associated proteins interesting as potential

therapeutic targets [Cantor et al., 2008].

3.1.3 Integrin activation and signaling

Integrins can be found in two different conformations. In a bent conformation integrins are inactive, due to the fact that the ligand-binding site is directed towards the cell membrane. Mn^{2+} is known as a positive regulator of the receptors and promotes a straightening of the extracellular domain between the head- and the tailpiece of integrins. In this extended conformation, $\alpha_v\beta_3$-integrins were shown to have an increased binding affinity to their ligands [Takagi and Springer, 2002].

Figure 3.4 depicts schematically the two conformational states of integrins.

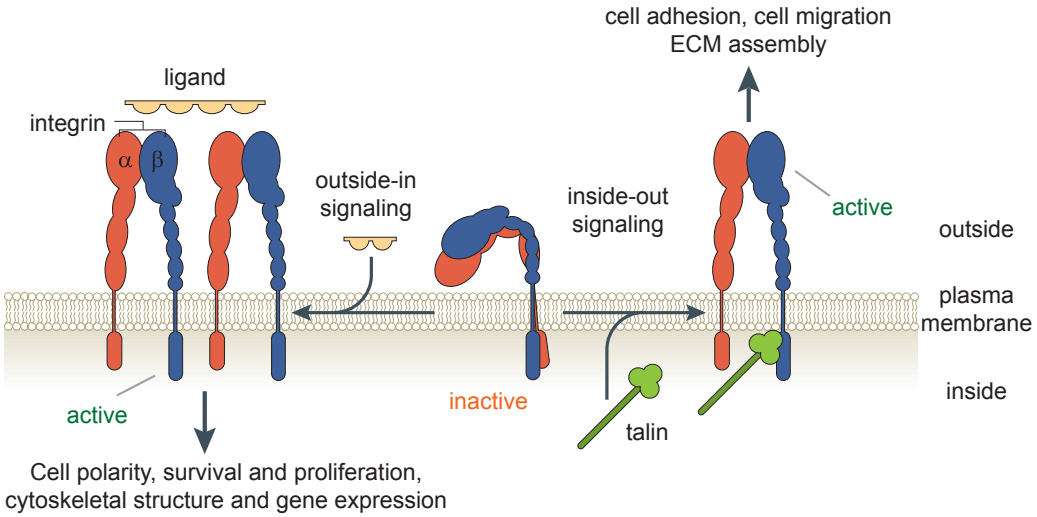

Figure 3.4: **Bidirectional integrin signaling.** Schematical representation of integrin activation from an inactive, folded (middle) to an active, stretched (left and right) conformation. In their active state, integrins regulate intracellular as well as extracellar processes. (Adapted from Shattil et al., 2010)

The activation of integrins is regulated by intracellular proteins that bind to the cytoplasmic β tail of integrins, increasing their affinity for ECM binding partners [Calderwood, 2004]. Talins and kindlins were shown to play a crucial role in this modulation [Shattil et al., 2010] .

3.2 Extracellular matrix

The space between tissue cells of multicellular animals is filled with extracellular matrix (ECM), a meshwork of proteins and polysaccharides, produced mainly by the cells surrounded by it. The ECM provides physical scaffolding for the cells embedded and serves as a reservoir of soluble molecules, such as growth factors. In connective tissue, cartilage and bone, the ECM is the functional part of the tissue, while in others, e.g. muscle, it only represents a minor portion. Depending on the type of matrix, ECM components can vary significantly.
One of the forms of the ECM is the so-called basal lamina, which underlies epithelial cell sheets and individual muscle cells, fat cells and Schwann cells. Basal laminae are usually 40-120 nm thick and not only have structural and filtering roles but also affect cell survival, proliferation or differentiation, polarity, migration and influence cell metabolism [Alberts et al., 2002].
ECM macromolecules can be subdivided into two classes: 1) glycosaminoglycans (GAGs) and 2) fibrous proteins.
GAGs are linear chains of 20 100 sulfated disaccharides that are usually linked to proteins, forming proteoglycans. Their high density of negative charges attracts cations, specially Na^+ making them highly hydrophilic. In connective tissues, they therefore form hydrated gels. Hyaluronan, chondroitin sulfate, dermatan sulfate, heparan sulfate and keratan sulfate are counted among GAGs.
The major proteins of the ECM are collagens, which are secreted by connective tissue cells. They represent the most abundant proteins in multicellular animals, where they constitute 25% of the total protein mass. Collagens are rich in proline - which stabilizes the helical conformation in each α chain - and in glycine - which, due to its small size, allows the helical chains to pack tightly together. Collagens are known to spontaneously form fibrils *in vitro*. However, their assembly *in vivo* is a cell-dependent process. The polymerization of collagen type I requires the presence of collagen V, collagen-binding integrins and fibronectin [Kadler et al., 2008].
Elastin, a highly hydrophobic protein, is the main component of the group of elastic fibers. It is, like collagen, rich in proline and glycine and is about

750 aminoacids long.
Basal laminae consist mainly of collagen type IV and laminin, a multiadhesive protein that binds not only collagen IV, but also certain CAMs.

3.2.1 FN types

Fibronectin (from the Latin: *fibra*, fiber, and *nectere*: to bind, tie) is a key component of the ECM. It provides binding sites not only for cell membrane receptors but also for other ECM proteins. It can be found in two forms that differ in their molecular composition, solubility and cellular source. Both types of the protein are encoded in one gene and result from alternative splicing [Kornblihtt et al., 1996].
In connective tissues and basal laminae FN is present as a fibrillar network, referred to as "cellular FN" (cFN). This form is produced mainly by fibroblasts, which deposit it locally and assemble it into an insoluble matrix.
The other physiologically ocurring type of the protein is plasma FN (pFN). This form is secreted by hepatocytes and released in a globular, inactive form into the plasma, where it circulates at a concentration of 300-400 μg/mL. It is therefore referred to as "plasma FN" (pFN) and can be incorporated into the ECM [Moretti et al., 2007].
It has been shown that the presence of cFN in plasma is increased in diseases, such as rheumatoid vasculitis and diabetes [Kanters et al., 2001]. One functional difference between the two types of the protein was observed by Asaga et al. [Asaga et al., 1991], who showed that human skin fibroblasts required cFN but no pFN for collagen gel contraction, which was suppressed after inhibition of protein biosynthesis.
In wound healing, the two types are temporally regulated. In a first step, the soluble pFN is incoroprated into fibrin clots regulating platelet function and hemostasis. Afterwards cFN is synthesized and assembled by cells migrating into the clot, thus reconstituting the damaged tissue [To and Midwood, 2011].

3.2.2 FN structure

FN is a glycoprotein consisting of two nearly identical monomers linked to each other by disulfide bonds. Each chain has a mass of approx. 250 kDa, is 60-70 nm long and 2-3 nm thick.
FN is a modular protein composed by three types of domains, referred to as type I, II and III [Wierzbicka-Patynowski and Schwarzbauer, 2003], which differ in tertiary structure and biological function. Figure 3.5 depicts schematically the modular structure of a FN monomer.

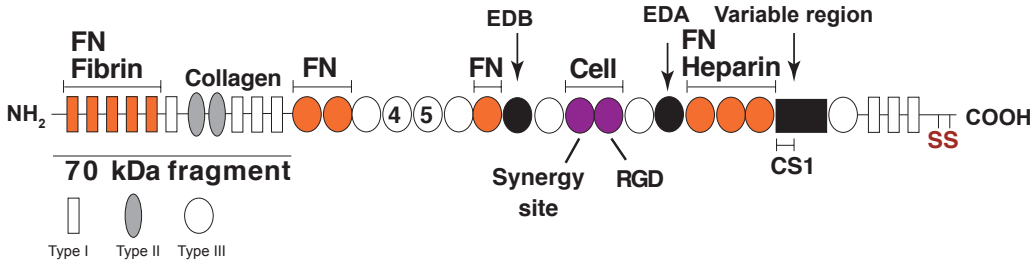

Figure 3.5: **The modular structure of fibronectin.** FN monomers consist of type I (rectangular), type II (oval) and type III (circular) domains. FN binding sites are colored in orange and the central cell binding domain containing the RGD and its synergy site PHSRN are shown in magenta. (Adapted from Wierzbicka-Patynowski and Schwarzbauer, 2003)

One of the major cell-binding domains present in all types of FN contains an RGD (Arg-Gly-Asp) sequence within $FNIII_{10}$ that promotes cell adhesion mediated mainly by the $\alpha_5\beta_1$-integrin. The RGD is bound primarily by the β subunit, while residues outside this sequence are believed to interact with the α subunit, affecting binding specificity and affinity [Takagi, 2004]. The aminoacid sequence PHSRN (Pro-His-Ser-Arg-Asn) in $FNIII_9$ was identified to act synergistically with the neighbouring RGD site enhancing its cell-adhesive function [Aota et al., 1994, Grant et al., 1997].
The extra domains EDA and EDB are alternative splicing sites within the FN gene that are only expressed in cFN [Kornblihtt et al., 1996]. EDA can be included between III_{11} and III_{12}, whereas EDB can be found between III_6 and III_7. EDA promotes cell adhesion of some cell types and it has a synergistic activity with the adjacent domains III_{11} and III_{12}. It further seems

to participate in signal transduction through the induction of stress fibers and focal contact assembly. In some cell systems, EDA containing FN is more effective in promoting cell spreading and migration than FN lacking it. A possible explanation for this behavior is the higher avidity of $\alpha_5\beta_1$-integrins to the first form [Manabe et al., 1997]. EDA was also identified as a ligand for integrins $\alpha_9\beta_1$ [Shinde et al., 2008], $\alpha_4\beta_1$ [Liao et al., 2002] and $\alpha_4\beta_7$ [Kohan et al., 2010].
The expression of EDA-containing FN is highly regulated during development and aging. The EDA exon was also shown to be necessary for a normal function of the brain [Chauhan et al., 2005].
Four FN binding domains have been identified, being FNI_{1-5} essential for assembly [Mao and Schwarzbauer, 2005a]. Other intramolecular ionic interactions are important for keeping FN in a compact form, unable to form fibrils in solution [Johnson et al., 1999]. Further domains bind other ECM components including collagens, fibrin, and various proteoglycans.

3.2.3 FN fibrillogenesis

Although FN assembly has been extensively studied, the mechanisms underlying this complex process remain widely unclear.
The protein is secreted in its globular, inactive form. Integrin-mediated cell binding induces conformational changes that allow the exposure of cryptic FN-FN binding sites, thereby inducing FN polymerization into fibers [Ingham et al., 1997].
It has been shown that a tensin-dependent translocation of $\alpha_5\beta_1$-integrins, the major FN receptor, promotes early FN fibrillogenesis [Pankov et al., 2000]. Cytoskeletal tension and cell traction forces are required for FN matrix assembly [Baneyx et al., 2002], and that these forces are largest at the cell periphery and decrease toward the cell center [Lemmon et al., 2009]. Taken together, as FN-ligated integrins translocate along actin filaments in centripetal direction, they apply tension to FN, thereby stretching it into its fibrillar, active form [Brown and Discher, 2009].
The main steps of FN assembly are depicted in figure 3.6.

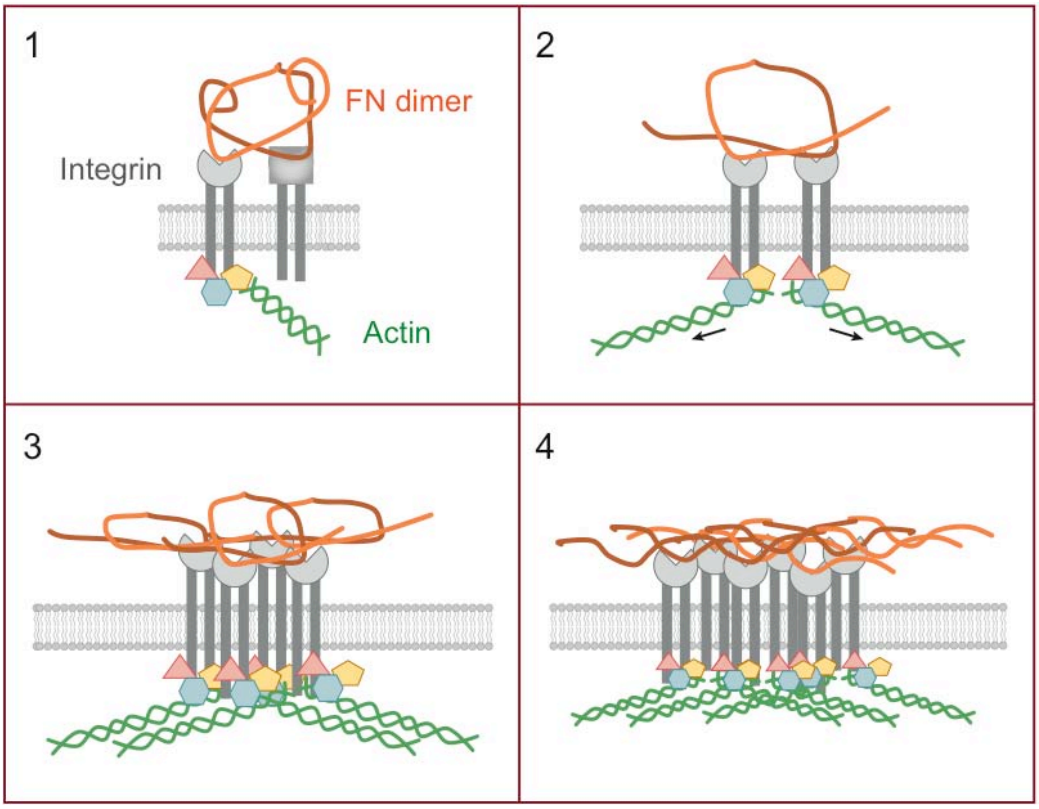

Figure 3.6: **Principal steps in the process of FN assembly. 1)** Globular FN (orange) binds integrins (gray). **2)** Intracellular proteins are recruited to the cytoplasmic domains of integrins and connected to the actin cytoskeleton (green). As cell contractility increases (arrows), FN undergoes conformational changes. **3)** Integrins cluster, binding and inducing conformational changes in further FN molecules. **4)** The exposure of cryptic FN-FN binding sites allows the polymerization of the protein into an insoluble matrix (adapted from Singh et al., 2010).

Different studies have shown that cytoskeletal tension is needed to unfold the dimer [Zhong et al., 1998, Pankov et al., 2000] and to maintain it in a partially unfolded conformation [Baneyx et al., 2002]. In the majority of stretched dimers, at least one FNIII is unfolded, allowing the whole molecule to extend up to 8-fold [Klotzsch et al., 2009].
The importance of FN organization is emphasized by several reports showing that an active FN matrix assembly is required for the incorporation of other molecules into the ECM, such as fibrillin [Sabatier et al., 2009], fibrinogen [Pereira et al., 2002] and collagen [Kadler et al., 2008]. Also os-

teoblast mineralization depends on β_1 integrin dependent FN deposition [Brunner et al., 2011].
Mao and Schwarzbauer have shown 3D extracellular matrix networks stimulate fibril assembly compared to 2D culture, suggesting effects of the 3D FN matrix on integrin activity [Mao and Schwarzbauer, 2005b]. These results were supported by Midwood et al., who showed that different conformations of FN activate distinct types of integrins [Midwood et al., 2006]. While soluble FN is bound by $\alpha_5\beta_1$-integrin, in its multimeric form it also stimulates $\alpha_v\beta_3$-integrin [Huveneers et al., 2008].

3.3 Biomimetic surfaces as a tool to study cell adhesion

Different *in vitro* approaches were developed in order to mimic *in vivo* adhesive environments. These span from glass coatings to artificial 3D matrices presenting ECM proteins or ECM-derived peptides. FNs, as integrin-ligands, are widely used as a cell-adhesive coating. Due to its easier availability and lower cost, pFN is the type that is utilized more often. Nevertheless, cFN also has adhesive properties and is the actual type of the dimer that promotes cell-adhesion *in vivo*. In some cell systems, moreover, cFN was shown to promote a faster spreading than pFN [Zand et al., 2003]. The physical properties of a substrate coating can be varied in order to study their effect on cell adhesion. It was reported that the physical state of FN on a glass surface plays a role on cell adhesion and FN assembly. While physisorbed pFN promoted matrix reorganization and $\alpha_5\beta_1$-integrin localization to fibrillar adhesions, a more rigid FN coating inhibited FN fibrillogenesis and it induced the formation of FAs rich in $\alpha_5\beta_1$-integrins [Katz et al., 2000].

3.3.1 Peptide immobilization on nanopatterned substrates

The covalent immobilization of cell-adhesive peptides offers advantages over protein adsorption. Physisorbed proteins not only can be degraded by proteases but also their orientation and availability cannot be controlled. One of the most employed peptides to induce cell adhesion is the RGD sequence, which occurs in different ECM proteins, such as fibronectin, vitronectin and fibrinogen [Humphries et al., 2006].
Modified peptides can be either directly covalently linked to substrates or indirectly coupled using different linkers. His-tagged proteins, for example, can be bound to Ni^{2+} ions. These, in turn, can be immobilized by chelation to NTA (nitrilotriacetic acid) bound to a surface [Knecht et al., 2009].
The immobilization can be carried out either homogeneously on an entire surface or on patterned substrates, where ligands are presented separated from each other in defined distances [Lohmüller et al., 2011]. Nanopatterned

substrates functionalized with cyclic RGD peptides can be used to control lateral $\alpha_v\beta_3$-integrin clustering [Arnold et al., 2004]. It was shown that fibroblast can form stable FAs on nanopatterned substrates presenting a critical inter-ligand spacing or lower. When this spacing is increased, not only adhesion is compromised, but also the synthesis of ECM proteins is affected [Cavalcanti-Adam, 2005].

3.4 Aim of the study

The aim of this study is to analyze fibroblast adhesion *in vitro* on substrates presenting cFN, pFN and peptides derived from FN.
While it is known that the two physiologically ocurring FN types exert different adhesive responses in some cell systems, it has not been studied how they regulate the formation of adhesion sites and FN fibrillogenesis.
In this work the formation of FAs and FBs was investigated in fibroblasts, the major cell type present in connective tissues involved in secretion and assembly of FN. The investigation focussed on the following aspects:

- The regulation of cell spreading by cFN and pFN.
- The molecular composition of FAs on cFN and pFN.
- The effects of FN coatings on integrin distribution and phosphorylation of paxillin - a major regulator of FN signaling.
- The effects of FNs and adhesive peptides derived from FN on the assembly of FN.

4 Materials and methods

The aim of this work is the characterization of fibroblast adhesion to different types of fibronectin (FN). For this purpose, we used surface coatings of cellular FN (cFN) produced by fibroblasts, plasma FN (pFN) secreted by hepatocytes and superfibronectin (sFN) which results from the *in vitro* mixture of pFN and the FN fragment $FNIII_{1-C}$ -also known as anastellin. Due to inconsistencies in the results obtained on sFN coatings, the investigations were restricted to cFN and pFN and only experiments on the two latter types of FN are shown in this thesis.

4.1 Preparation of homogeneous substrates

4.1.1 Direct physisorption of FNs on glass

Glass coverslips (Carl Roth) were incubated for 1 hr at 37°C or overnight at 4°C with 5 μg/mL cFN, pFN or sFN solution in PBS.
cFN (Sigma) from human foreskin fibroblasts was supplied as lyophilized powder in CAPS (3-(cyclohexylamino)-1-propanesulfonic acid) saline buffer. After reconstitution in Milli-Q water, the protein concentration was determined using a BCA (bicinchoninic acid) assay kit (Thermo Scientific) and aliquots were stored at -20°C.
For the isolation and purification of human pFN, human serum was centrifuged and after addition of 2 mM PMSF and 10 mM EDTA it was purified using a Sepharose column. FN was eluted with PBS/6M Urea and the eluate was dialyzed against PBS. The protein concentration was determined using the BCA assay. Aliquots were stored at -20°C.
Bovine pFN (Sigma) was supplied in solution in 0.5 M NaCl, 0.05 M Tris (Roth), pH 7.5 and stored at 4°C.
BSA (bovine serum albumin, Sigma, 1 % (w/v) in PBS, sterile filtered) was used in order to prevent unspecific cell binding. The FN coated substrates were incubated for 30 min at RT with this solution in order to block parts of the glass surface which might not have been coated with FN.

4.1.2 Indirect physisorption of FNs on glass

Glass coverslips were incubated for 20 min with 50 μg/mL PLL (poly-L-lysine, Sigma), rinsed with Milli-Q water and incubated with 1 % glutaraldehyde (Sigma) for 15 min at RT. After extensive washing the coverslips were incubated for 30 min with 5 μg/mL FN, washed and blocked with 1M ethanolamine (Sigma) in PBS for 20 min [Katz et al., 2000].

4.1.3 Immobilization of cRGDfK on gold surfaces

After 30 min incubation with a 3:1 mixture of H_2O_2 and H_2SO_4 (both from Carl Roth) and extensive washing with Milli-Q water, glass slides were sputtered with a 4 nm thick layer of titanium and a 10 nm thick layer of gold in the chamber of a modular high vacuum coating unit (BAL-TEC Med 020). The surfaces were then incubated with a 25 μM solution of the cyclic pentapeptide c(Arg-Gly-Asp-Phe-Lys) (cRGDfK) for 4 hr at RT. To prevent the

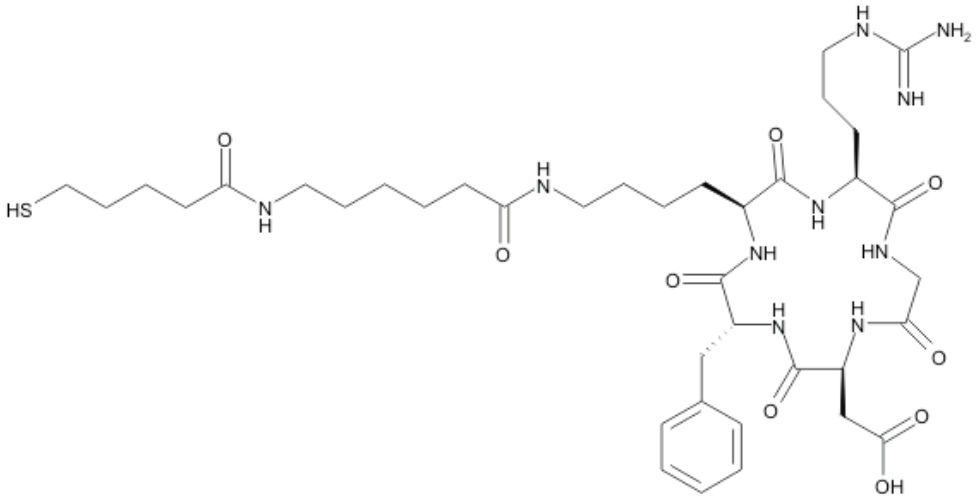

Figure 4.1: **Chemical structure of the cyclic RGD** (cRGDfK) including a linker with a terminal thiol group that can be covalently bound to the gold surfaces. cRGDfK was kindly provided by Prof. Dr. Kessler, TU Munich.

deposition of organic material on the surfaces, the incubation was performed immediately after sputtering or following plasma treatment (t = 10 min, p[O_2] = 0.4 mbar, p = 150 W).
Prior to cell seeding the substrates were rinsed extensively with Milli-Q water and finally with sterile PBS.

4.1.4 Immobilization of FN-fragments on gold surfaces

A fibronectin fragment $FNIII_{9-10}$ [Staunton et al., 2009] (kindly provided by David Staunton, Department of Biochemistry, University of Oxford) was reconstituted in Milli-Q water, aliquoted and stored at -20°C (figure 4.2).

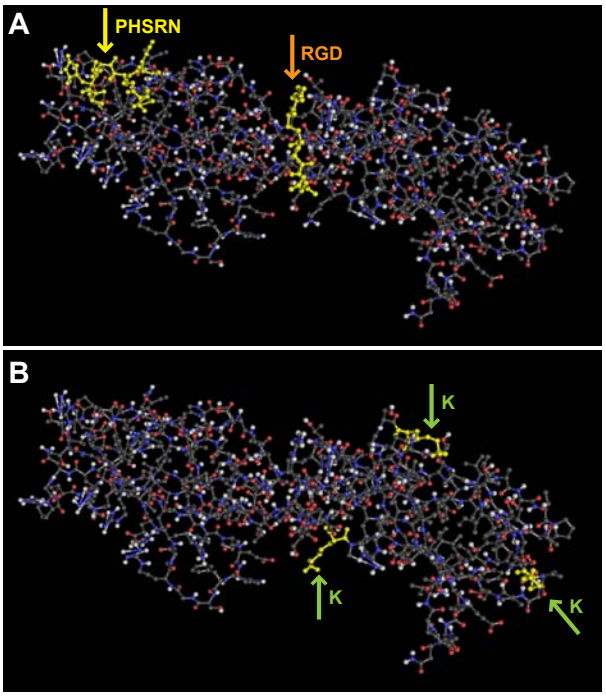

Figure 4.2: **3D structure of $FNIII_{9-10}$.** Both boxes show $FNIII_{9-10}$. In box A the synergy site PHSRN (Pro-His-Ser-Arg-Asn) in $FNIII_9$ is indicated with a yellow arrow and the cell-binding tripeptide RGD within $FNIII_{10}$ with an orange arrow. In box B green arrows point at the three lysines present in the fragment, which are accessible for Traut's Reagent.

The thiolating Traut's Reagent (2-Iminothiolane*HCl, Thermo Scientific)

was used for the immobilization of $FNIII_{9-10}$ to gold. The reagent interacts with primary amines (-NH_2), introducing thiol (-SH) groups (figure 4.3).

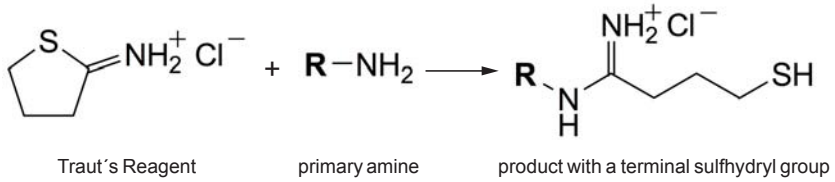

Figure 4.3: **Chemical reaction between Traut's Reagent and primary amines.** The compound reacts with primary amines resulting in a product containing a terminal sulfhydryl group.

5 mM EDTA was added to 1 mg/mL $FNIII_{9-10}$ to chelate divalent metal ions in order to prevent the oxidation of -SH groups. An approx. 10-fold molar excess of Traut's Reagent dissolved in PBS was added to the protein solution. After 1 hr incubation at RT, glass coverslips previously sputtered with a 4 nm thick layer of titanium and 10 nm gold were incubated with the solution for an additional hour at RT. The substrates were rinsed with PBS under sterile conditions prior to cell seeding.

4.2 Preparation of nanopatterned substrates

Nanopatterning of glass substrates was done according to Arnold et al., 2004. Polystyrene(x)-*block*-poly(2-vinylpyridine)(y), PS(x)-*b*-P2VP(y) (Polymer - Source), is dissolved in toluene or para-xylene. This results in a micellar solution, where PS forms the outer shell of the micelles. When $HAuCl_4$ (Sigma) is added to this solution, it diffuses into the micelles, protonating the P2VP while the negatively charged Au(III) complex $AuCl_4$ stabilizes the micellar core. When a solid inorganic surface, e. g. a glass coverslip, is retracted from the solution after dip-coating, the gold-loaded micelles adsorb onto the surface building a self assembled monolayer (SAM), where gold particles are organized in a quasi-hexagonal pattern. The interparticle distance can be varied depending on the polymer length and the velocity at which the surface is retracted from the micellar solution [Arnold et al., 2004]. The diameter of the gold particles is determined by the loading, which is the molar ratio between $HAuCl_4$ and the sum of all P2VP units. The solutions of diblock copolymers used to obtain the different distances between neighbouring gold clusters are listed in table 1.

Table 1: **Polymers used for the production of nanopatterns.** The amount of polymer units is indicated in brackets. MW: molecular weight of the diblock copolymer, c: concentration of the polymer, L: loading or molar ratio between $HAuCl_4$ and P2VP, d: interparticle distance.

Polymer	MW [g/mol]	c [mg/mL]	L	d [nm]	solvent
PS(240)-*b*-P2VP(143)	40000	8	0.5	30	para-xylene
PS(1056)-*b*-P2VP(495)	162000	5	0.5	53-80	toluene
PS(2076)-*b*-P2VP(571)	276000	2	0.5	110	toluene

Polymer was dissolved in toluene or para-xylene (Merck) and stirred at least for 24 hr. The polymer solution was then added to the $HAuCl_4$ and stirred for at least 24 hr at RT until the salt was completely dissolved. The solution was stored at RT protected from light and was used within six months after preparation.

4.2.1 Dip-coating and plasma etching

Glass coverslips were cleaned with lint-free napkins and immersed in a 3:1 mixture of H_2SO_4 and H_2O_2 for 30 min. After repeated rinsing with Milli-Q-water, the coverslips were sonicated for 5 min, rinsed again and dried with a nitrogen stream. After dipping in the micellar solution, the glass coverslips were treated with hydrogen plasma ($t = 45\,min$, $P = 300\,W$, $p[H_2] = 0.4\,mbar$, PS 210 Microwave Plasma System or $t = 45\,min$, $P = 150\,W$, $p[H_2] = 0.4\,mbar$ in PS 100-E, both from TePla) in order to remove the polymers on the surfaces and reduce Au(III) to Au(0).

4.2.2 Passivation of glass surface

The nanopatterned coverslips were subjected to passivation with biologically inert poly(ethylene glycol) (PEG). The polymer binds to the glass surface between gold clusters and on the part of the sample that was not immersed in the gold solution [Blümmel et al., 2007]. The basic structure of PEG is $HO(\text{-}CH_2\text{-}CH_2\text{-}O)_n\text{-}H$.
In this work a silane terminated PEG2000-carbamate (n = 43, shown in figure 4.4) was used to passivate the surfaces. PEG was prepared and kindly provided by Dr. J. Blümmel or T. Pohl.

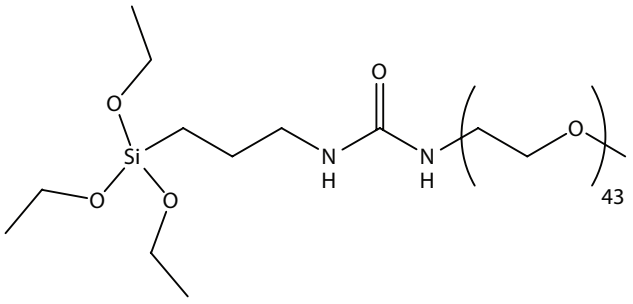

Figure 4.4: **Structure of PEG2000-carbamate.** Silane-terminated, protein repellent PEG2000-carbamate used to passivate the glass surface between the gold particles.

The substrates were immersed for 8 hr at 80°C in a 0.25 mM PEG2000-carbamate solution in dry toluene and 2.5 μM triethylamine (Fluka), which acts as a catalyst. After removal of the toluene, the substrates were rinsed

three times with ethylacetate and then with methanol (both p.A., from Carl Roth). After nitrogen drying, the surfaces were ready for biofunctionalization with peptides.

4.2.3 Immobilization of peptides on gold particles

Immediately after the passivation with PEG, the substrates were incubated with either cRGDfK for 4 hr at RT or $FNIII_{9-10}$ for 1 hr at RT after incubation with Traut's Reagent as described in paragraphs 4.1.3 and 4.1.4.

4.3 Characterization of FN solutions and coatings

4.3.1 SDS-PAGE and Coomassie staining

1 μg protein was loaded onto a 4-12 % Bis-Tris Novex gel (Invitrogen) for SDS-PAGE (sodium dodecylsulfate - polyacrylamide gel electrophoresis) analysis. After electrophoresis (in MOPS buffer, t = 50 min, U = 200 V, I = 110 mA) the gel was incubated in 0.1 % Coomassie R-250 (Invitrogen) in 40 % ethanol (AppliChem) and 10 % acetic acid and heated for 1 min in a microwave oven (P = 300W). It was then gently shaken at RT for 15 min and rinsed once with Milli-Q water after removing the excess stain. The gel was heated for 1 min in a solution containing 10 % ethanol and 7.5 % acetic acid for destaining. Images were acquired with the luminescent image analyzer LAS-3000 (FUJIFILM).

4.3.2 Chemiluminescence detection of FN in solutions

0.5 μg of each protein solution was analyzed by SDS-PAGE using 4-12 % Bis-Tris pre-cast gels with NuPAGE system (Invitrogen). After electrophoresis (in MOPS buffer, 50 min, 200 V, start current 110 mA) proteins were transferred to a nitrocellulose membrane using iBlot Dry Blotting System (Invitrogen). The membrane was blocked for 1 hr at RT with 5 % milk (Carl Roth) in PBS and incubated overnight at 4°C with primary antibody against EDA or vitronectin (see 3) diluted to a final concentration of 0.1-0.5 μg/mL in PBS-T containing 3 % milk. The nitrocellulose membrane was washed three times with PBS-T for 5 min, incubated for 45 min with HRP-conjugated secondary antibody in PBS-T/3 % milk at a final concentration of 0.1 μg/mL and rinsed three times with PBS-T for 5 min.
The proteins on the nitrocellulose membrane and on the glass substrates were detected by chemiluminescence (ECL Plus, Amersham Corp.) and imaged with the luminescent image analyzer LAS-3000 (FUJIFILM).

4.3.3 *In situ* detection of proteins on FN coatings

Glass coverslips were coated and blocked as described in paragraph 4.1.1 and incubated for 1 hr at RT with primary antibody against FN, EDA or vitronectin (see 3). After rinsing with PBS, substrates were incubated for 45 min in HRP-conjugated anti-mouse antibody (see 4), rinsed with PBS and the proteins were detected by chemiluminescence as described in paragraph 4.3.2.

4.3.4 Fluorescence labeling of FN

Bovine pFN was labeled using AlexaFluor 555 Protein Labeling Kit (Invitrogen). The dye has a succinimidyl ester moiety that reacts efficiently with primary amines. Since pFN was supplied in TRIS, which contains an amino group, it was first dialyzed against PBS. The protein solution was transferred to a vial of reactive dye. The reaction mixture was stirred for 1 hr at RT. The labeled FN was purified with a purification column provided in the labeling kit. The protein-containing fraction was collected and the concentration was measured by UV-VIS-spectra on an Tecan InfiniteM200 microplate reader (Tecan).

4.3.5 Quartz Crystal Microbalance with Dissipation

Quartz crystals (L.O.T.-Oriel GmbH & Co. KG) were subjected to oxygen plasma treatment (t = 30 min, P = 150 W, p[O_2] = 0.4 mbar) and mounted into an E4 sensor system from Q-Sense. The deposition of FN was monitored on silicon dioxide coated crystals (Q-Sense). The adsorption of His-tagged FN fragments was measured on gold crystals (QS-QSX301, Q-Sense). The baseline frequency and dissipation level of buffers were determined before the addition of proteins or linkers. The solutions were pumped into the chambers with a velocity of 50 μL/min. Once the chambers were filled with the protein solution, the pump was stopped and frequency and dissipation level were measured until an equilibrium was reached. The average mass adsorption,

dissipation level and corresponding standard deviation were calculated using values within 10 min after reaching constant levels.

4.3.6 Scanning Electron Microscopy

The gold-nanopatterned surfaces were analyzed after plasma treatment with scanning electron microscopy (SEM). Samples were coated with a layer of carbon in the chamber of a sputter coater (BAL-TEC MED 020) and imaged with SEM (Leo1530, Zeiss). A 50.000 magnification was used to analyze spacing and order of the gold particles applying the "dot analyzer" plugin created by Dr. Philippe Girard for ImageJ. This plugin measures the average distance between neighbouring gold particles and standard deviation. It also gives an order parameter ranging from 0 to 1 where 1 represents a perfect order. Only nanopatterns yielding an order parameter above 0.6 were used for cell experiments.

4.4 Cell culture

4.4.1 Cell lines and culture conditions

Wild type rat embryonic fibroblasts (REF52WT), REF52YFPpax (REF stably transfected for the expression of YFP-tagged paxillin), 3T3YPet-FN and CDP (cells of the dental pulp) cells were cultured in Dulbecco's Modified Eagle's Medium (DMEM, Gibco) supplemented with 1 % L-Glutamin and 10 % serum (Gibco) and were used at passages 5-20. Cells were serum-starved for 16 hr before the experiments.
Every three days the media was replaced. When the cells were confluent (4-7 days after plating) the media was removed and the cell monolayer was first rinsed with PBS (PAA) to remove residual media and then incubated for 3 min with 2.5 % Trypsin/EDTA (Gibco). Once the cells detached, media supplemented with 10 % FBS or FCS (fetal bovine serum or fetal calf serum, see table 2) was added to the flask to neutralize the trypsin. The cell suspension was centrifuged for 5 min at 800 rpm. The pellet was resuspended in culture media and cells were seeded 1:10 into a new flask.

Table 2: Cells

Name	Organism	Serum	Description	Reference
REF52WT	rat	FBS	fibroblast	[Franza et al., 1986]
REF52YFPpax	rat	FBS	transfected fibroblast	[Zamir et al., 1999]
CDP	human	FBS	cells of the dental pulp	[Waddington et al., 2009]
3T3YPet-FN	mouse	FCS	transfected mouse fibroblast	[Ohashi and Erickson, 2009]
MEF $FN^{-/-}$	mouse	no serum	transfected mouse fibroblast	[Fässler et al., 1995, Sakai et al., 2001]
MEF $FN^{fl/fl}$	mouse	FCS	transfected mouse fibroblast	[Fässler et al., 1995, Sakai et al., 2001]

MEF $FN^{-/-}$ were first thawed and cultured in DMEM supplemented with 10 % FBS. After the second passage, the culture media was replaced with a 1:9 mixture of this media and serum-free media. After two passages, cells were cultured in serum-free media on Petri dishes precoated with 50 $\mu g/\mu L$ type I collagen (BD Biosciences) in 0.02 N acetic acid. Serum-free media was prepared as follows: 500 mL AimV (Gibco), 500 mL DMEM/HAM'SF-12 (PAA), 20 mL RPMI 1640 (Gibco) and 10 mL NEAA (non-essential amino-acids, Gibco).

4.4.2 Mycoplasma test

For each passage after thawing and then bimonthly, the absence of parasitic mycoplasm in the cell culture was tested. Approximately 30.000 cells were incubated in 2 mL 10 %-DMEM for 24 hr in a Petri dish. After media removal, cells were fixed with 70 % ice-cold methanol for 4 min. Cells were then incubated for 15 min in a 1 μg/mL DAPI (4, 6-diamidino-2-phenylindole, Sigma) solution. The substrate was rinsed with PBS and the presence of DNA-intercalating DAPI was detected by fluorescence microscopy.
The excitation of the dye is 359 nm, while its emission at 461 nm is enhanced by approx. 20-fold when bound to DNA. Mycoplasma infected cells show a characteristic particulate or filamentous staining on the cell surface.
Only mycoplasma-negative cells were used in this study.

4.4.3 Cell seeding

After trypsinization cells were centrifuged and resuspended in media supplemented with 1 % FBS or FCS. The cell titer was determined using a Neubauer chamber. 30.000 cells in suspension were seeded on each substrate. The plates were placed in the incubator until the time point of fixation. The remainder of the cell suspension was used for further passaging.

4.4.4 Cell transfection

For transient transfection and expression of fluorescent protein-constructs, REF cells were plated in 6-well plates, and allowed to reach 70-80 % confluence. Transfection was performed with Promofectin (PromoCell) according to manufacturer's recommendation.
The α_5-integrin-GFP plasmid was obtained from the plasmid bank Addgene (plasmid 15238); the plasmid was deposited by R. Horwitz (University of Virginia, USA).

4.5 Preparation of cell samples

4.5.1 Cell fixation and permeabilization

After removal of the culture media the samples were rinsed three times with warm PBS and incubated at RT with 3.7 % PFA (Sigma) for 30 min. In case of staining of intracellular components, cells were fixed for 15 min with 3.7 % paraformaldehyde (PFA) and permeabilized for 10 min with 0.1 % Triton X-100 in PFA. The samples were rinsed thoroughly with PBS.

4.5.2 Indirect immunofluorescence staining

Fixed cells were blocked with 1 % BSA in PBS for 30 min and incubated with primary antibody/antibodies in 0.1 % BSA in PBS for 1 hr at RT or overnight at 4°C. Primary antibodies are listed in table 3 and were used at a final concentration of 1-5 μg/mL. Samples were rinsed three times with PBS and incubated for 45 min at RT with secondary antibody/antibodies in 0.1 % BSA in PBS. For actin labeling, TRITC-conjugated phalloidin (Sigma) was added to the secondary antibody dilution to a final concentration of 2 μg/mL. Secondary antibodies are listed in table 4 and were used at a final concentration of 5-10 μg/mL.
After rinsing with PBS, each glass slide was placed on an object holder, coated with 80 μL mounting media (Elwanol), covered with a microscopy glass slide and stored protected from light to avoid photobleaching.

4.5.3 Protein isolation and Western blotting

After media removal, cells were first rinsed with warm PBS and then lysed for 15 min on ice. Lysis buffer contained 20 mM Tris-HCl buffer (Biomol), 1 % NP-40, 150 mM NaCl (Grüssing), 1 mM EGTA, 1 mM sodium orthovanadate, protease inhibitors and 1 % deoxycholic acid, pH 8.0 (all from Sigma). The lysates were centrifuged at 14.000 rpm for 10 min at 4°C. Protein concentration in the supernatant was determined by BCA assay.

After addition of reducing agent and loading buffer, 4 μg of each sample were incubated for 10 min at 90°C. Proteins were analyzed by SDS-PAGE using 4-12 % Bis-Tris pre-cast gels with NuPAGE system (Invitrogen) as described in paragraph 4.3.2.

4.5.4 Lists of antibodies

Table 3: **Primary antibodies** WB: Western blotting, IIF: indirect immunofluorescence, CL: chemiluminescence

Epitope	Host	Catalogue number	Company	Application
β-actin	mouse	A2228	Sigma	WB
fibronectin (CCBD)	mouse	MAB1926	Millipore	IF, CL
fibronectin	mouse	42040	QED	IIF
fibronectin	rabbit	AB2047	Millipore	IIF
$FNIII_4$	mouse	F0791	Sigma	IIF
fibronectin, cellular	mouse	MAB1940	Millipore	IIF, CL, WB
phospho-paxillin^{pY118}	rabbit	2541S	Cell Signaling	IIF
phospho-paxillin^{pY118}	rabbit	AB3837	Millipore	WB
paxillin	rabbit	2542	Cell Signaling	IIF
vinculin	mouse	V9264	Sigma	IIF
vitronectin	mouse	MAB1945	Millipore	IIF, WB
zyxin	mouse	307011	Synaptic Systems	IIF

Table 4: Secondary antibodies

Name	Conjugation	Catalogue number	Company	Application
goat anti-rabbit IgG	HRP	sc-2004	Santa Cruz	WB
goat anti-mouse IgG	HRP	sc-2005	Santa Cruz	WB
goat anti-rabbit IgG	AlexaFluor 360	A-21068	Invitrogen	IIF
goat anti-rabbit IgG	AlexaFluor 488	A-11001	Invitrogen	IIF
goat anti-mouse IgG	AlexaFluor 647	A-21236	Invitrogen	IIF

4.6 Cell imaging and image processing

4.6.1 Epifluorescence Microscopy

The samples were observed with an Olympus IX inverted fluorescence microscope (Olympus) using a DeltaVision (DV) system (Applied Precision Inc.). The system is equipped with an incubation chamber for constant temperature (37°C) and 5 % CO_2 pressure thus allowing longer experiments with live-cells. A 20x air objective was used for phase microscopy. For all other samples a 60x oil immersion objective was used.

4.6.2 Total Internal Reflection Fluorescence Microscopy

For TIRF microscopy, fibroblasts were seeded on custom-made glass-bottom Petri dishes and imaged on a Nikon TIRF unit on a TE-2000 E (Nikon) using a 488- or a 561-nm laser line for excitation. An 60x PlanApo TIRF oil immersion objective NA 1.45 (Nikon) was used, and images were recorded with a Hamamatsu ORCA-AG digital camera at 1 Hz.

4.6.3 Image processing and data analysis

Image processing was done using ImageJ software version 1.43d (Rasband, W.S., ImageJ, U. S. National Institute of Health, Bethesda, Maryland, USA, http://rsb.info.nih.gov/ij/). Brightness and contrast of microscopy images were adjusted for the presentation.

ImageJ was used to assign colors to pictures of cells acquired with fluorescence filters and to generate RGB images by merging the different signals. The software was furthermore used to measure cell area in phase contrast images and to quantify bands of western blots.
Background subtraction was applied on the images using ImageJ. The program calculates the mean intensity of a selected ROI and subtracts the obtained value from each pixel within the image.
Intensity maps of integrin clusters were generated with ImageJ. The images were pseudocolored with the "spectrum" lookup table.
The velocity of the growth of single α_5-integrin clusters was determined by using the kymograph plugin written by J. Rietdorf and A. Seitz for ImageJ. Kymographs are assembled from a selected line type Region Of Interest (ROI) in each frame of a time series. In the resulting time-space-plot the y axis represents time and the x axis is the length of the ROI. The velocity of the growth of clusters was determined by measuring the slope of contrast edges in the kymographs.
The Intensity Correlation Analysis Plugin used to generate PDM (product of the difference from the mean) values and images was written by T. Collins and E. Stanley [Li et al., 2004].

5 Results

5.1 Characterization of FN solutions and of functionalized substrates

5.1.1 Surface adsorption of cFN was higher than that of pFN

Quartz crystal microbalance with dissipation (QCM-D) was used to analyze the deposition of proteins on surfaces. Therefore, frequency and dissipation levels of silicon dioxide coated crystals were monitored during incubation with the different solutions used for later cell experiments. While the calculated mass of cFN that adsorbed on the substrate was 555.2 ± 38.0 ng/cm^2, the value of adsorbed pFN was 332.6 ± 27.3 ng/cm^2 (figure 5.1). As expected, the

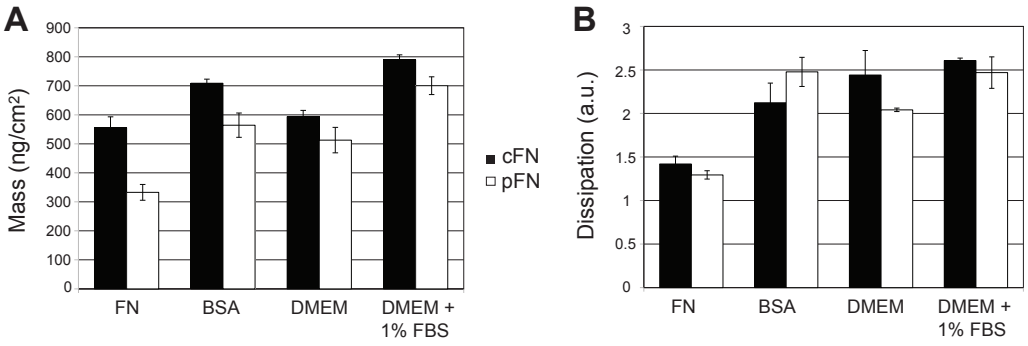

Figure 5.1: **Values of adsorbed mass and dissipation as calculated with QCM-D. A.** Total adsorbed mass after incubation with the indicated solutions. **B.** Dissipation levels of the protein coatings. Values on cFN are shown in black, pFN in white (n=3).

frequency level decreased after incubation with 1% BSA in PBS and rinsing with PBS, indicating an increase in the total amount of adsorbed mass. The mass calculated after further incubation with DMEM supplemented with 1% FBS and rinsing with PBS increased between 10 and 24%. In contrast, incubation of coated substrates with DMEM led to an increase in frequency levels, showing that proteins detached from the crystals. Figure 5.1 B shows that the measured dissipation levels did not vary significantly between the two different types of FN coatings, indicating that the amount of proteins deposited on the surfaces was not affected by the source of the protein.

5.1.2 FN solutions were free from vitronectin contamination

The total protein contents, within the FN solutions used for glass coatings, and, in FBS and DMEM used for cell experiments, were determined by SDS-PAGE and Coomassie staining (figure 5.2 A). To determine if vitronectin (VN), the major ligand for $\alpha_v\beta_3$-integrin, was present in the solutions, purified VN was loaded in the second lane and detected at 60 kDa. The lanes loaded with purified FNs in lanes 3 and 4 showed the expected bands for monomeric FN at approx. 230 kDa and a higher band representing polymeric FN. Further lower bands were detected in cFN. Several bands were found in FBS. There was no VN visible in DMEM.
The absence of VN in the solutions was further confirmed by western blot analysis (Figure 5.2 B).

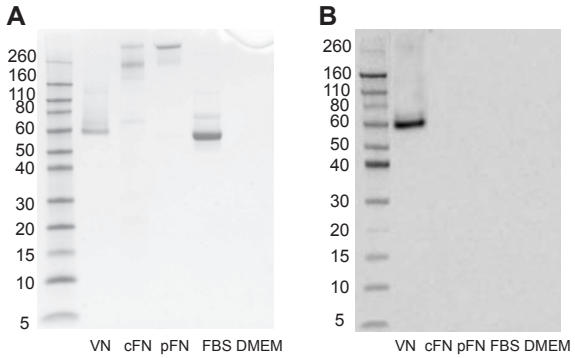

Figure 5.2: **Characterization of FN solutions. A.** The total protein content in solutions of purified vitronectin (VN) and FN, FBS and DMEM was stained with Coomassie. **B.** Western blotting showed VN contamination neither in FN solutions nor in culture media.

5.1.3 EDA was present in cFN and absent in pFN solutions

EDA is known to be present exclusively in cFNs and to affect the molecular conformation of the protein, thus influencing integrin specificity of the cell binding domain in $FNIII_{10}$ (RGD). Its presence in the extracts used for the coatings was determined by western blotting and *in situ* chemiluminescence

detection as described in 4.3.3.

Western blot analysis shown in figure 5.3 confirmed the presence of EDA in cFN. pFN was not contaminated with EDA-containing cFN.
Furthermore, coated glass substrates were tested for the accessibility of FNs and in particular EDA. Therefore, either FN, EDA or VN were detected on the different coatings previously incubated with DMEM or DMEM supplemented with 1% FBS. Figure 5.4 A shows that on directly physisorbed FNs, the protein was accessible to antibodies (top row), as well as EDA in cFN coatings (middle row). Contamination with VN was excluded as no chemiluminescence was detected after incubation with anti-VN antibody.

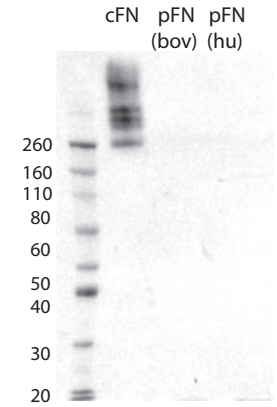

Figure 5.3: **Western blot of FN solutions.** EDA was detected exclusively in cFN.

In addition, figure 5.4 B shows the accessibility of EDA in cFN adsorbed on glass coverslips both directly (phys.) and indirectly physisorbed (ind. phys.) through glutaraldehyde on a PLL-layer.

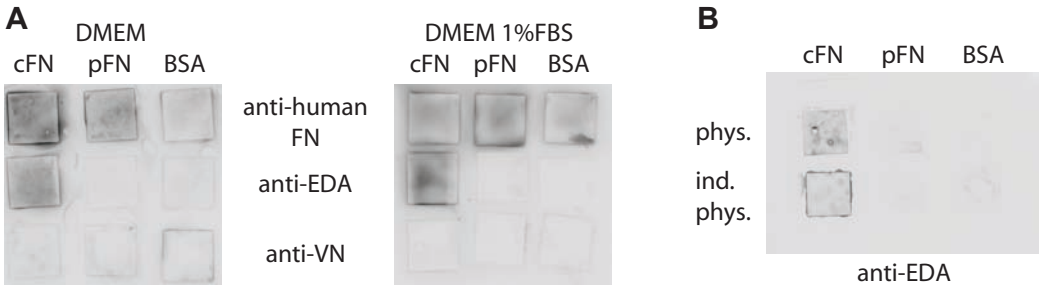

Figure 5.4: **Chemiluminescence detection of FN, EDA and vitronectin on FN coatings. A.** Detection of FN, EDA and vitronectin on glass coated with cFN, pFN or BSA after incubation with DMEM or DMEM supplemented with 1% FBS. **B.** Detection of EDA on directly and indirectly physisorbed FNs.

5.1.4 FNs adsorbed homogeneously on glass

In order to visualize the adsorbed FNs and to analyze how the distributed on glass, coverslips were coated with 5 μg/ml FNs prelabeled with Alexa-Fluor 555 (cFN_{555}, pFN_{555}), and imaged with fluorescence microscopy.
Figure 5.5 shows that FNs built a layer on glass, where they distributed homogeneously over the surface. No aggregations nor fibrils were observed on any of the samples.

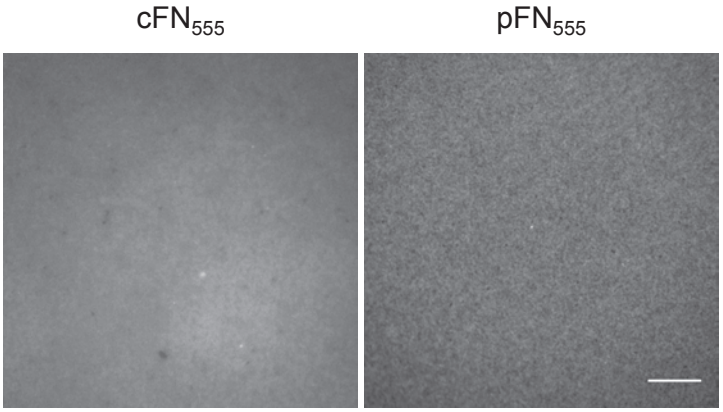

Figure 5.5: **Glass coatings with prelabeled FNs.** Glass coverslips were incubated with either cFN_{555} or pFN_{555} and imaged with fluorescence microscopy. (scale bar: 10 μm)

5.1.5 Production of nanopatterned glass surfaces

After the removal of the polymer with H_2 plasma treatment, nanopatterned glass coverslips were sputtered with a layer of graphite and imaged with SEM (scanning electron microscopy) using a 50,000 magnification. Figure 5.6 shows SEM images of samples presenting the four inter-particle distances used in this study.
The "dot analyzer" plugin for ImageJ (described in paragraph 4.3.6) was used to analyze the inter-particle distance as well as the order parameter, which ranged between 0.55 and 0.7 in all cases, where 0 represents no ordered

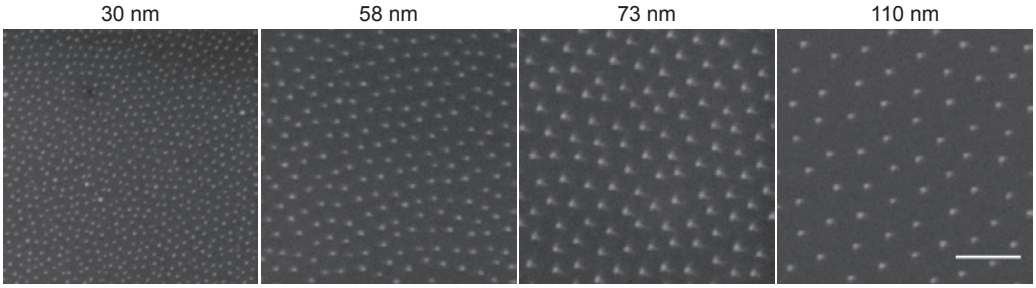

Figure 5.6: **Scanning electron microscopy images of gold nanoarrays.** Gold nanopatterned glass substrates were plasma treated to remove the polymer and imaged with a 50,000 magnification to analyze inter-particle distance and order parameter. The mean distance is indicated above each picture. (scale bar: 200 nm)

distribution and 1 indicates perfect order.

5.2 Fibroblast spreading on FN coatings

5.2.1 Cell spreading kinetics was similar on pFN and cFN

To rule out the effect of serum adhesive proteins, REF52WT cells were serum deprived for 16 hr prior to seeding onto coverslips coated with cFN or pFN. Non-coated glass coverslips were used as control (not shown). The progression of the projected cell area was monitored by time-lapse phase contrast microscopy for the initial 8 hr after seeding. Figure 5.7 A shows images of a representative cell on each type of surface at the time points indicated above. The projected cell area was measured and plotted (figure 5.7 B) as

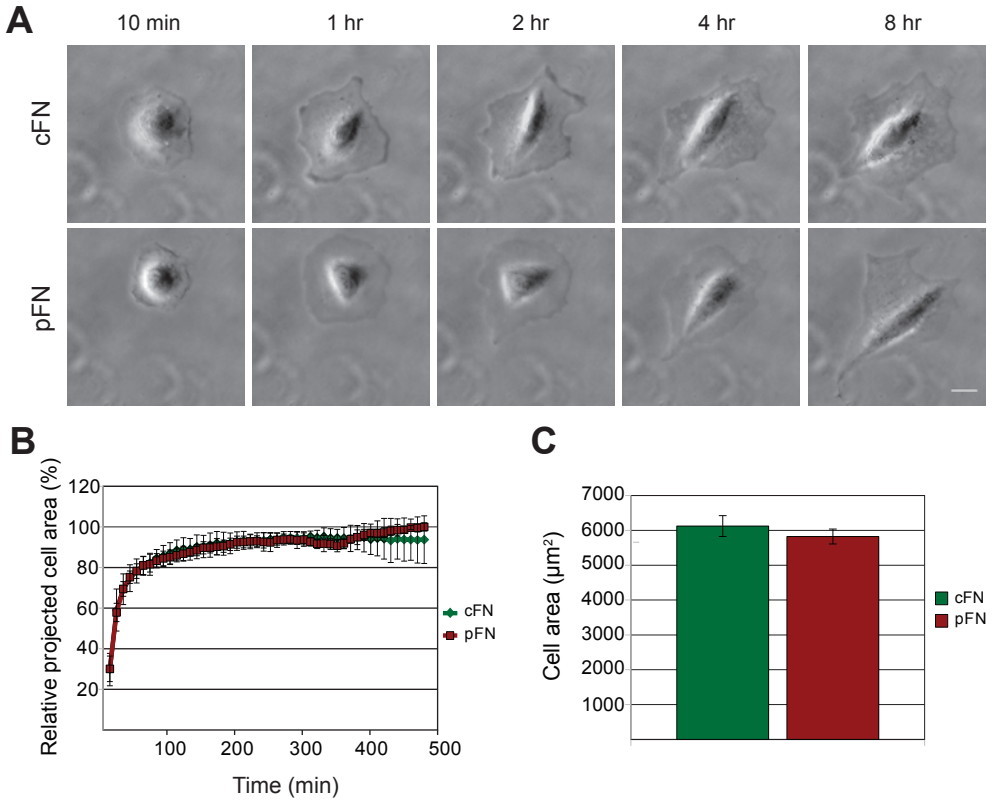

Figure 5.7: **Cell spreading kinetics of REF52WT cells on cFN and pFN coatings.** **A.** Phase contrast images show representative cells adhering on cFN and pFN. (scale bar: 20 μm) **B.** The graph shows the progression of the projected cell area relative to the maximal cell area. **C.** Bars show the mean cell area on the two substrates. (n=3)

percentage of the maximal value observed during the spreading phase.
cFN and pFN promoted initial cell spreading in comparison to glass. Here, the projected cell area increased linearly and reached a value that was approximately 50% of the maximal cell area compared to the values measured on FNs. On both types of FNs, spreading kinetics were nearly identical and the mean projected cell area did not differ significantly, as shown in figure 5.7 C. 18-23 cells per experiment were measured. Since the maximal area values were reached on all FN coatings after 4 hr, further experiments for the characterization of cell adhesion behavior were carried out at this time point.

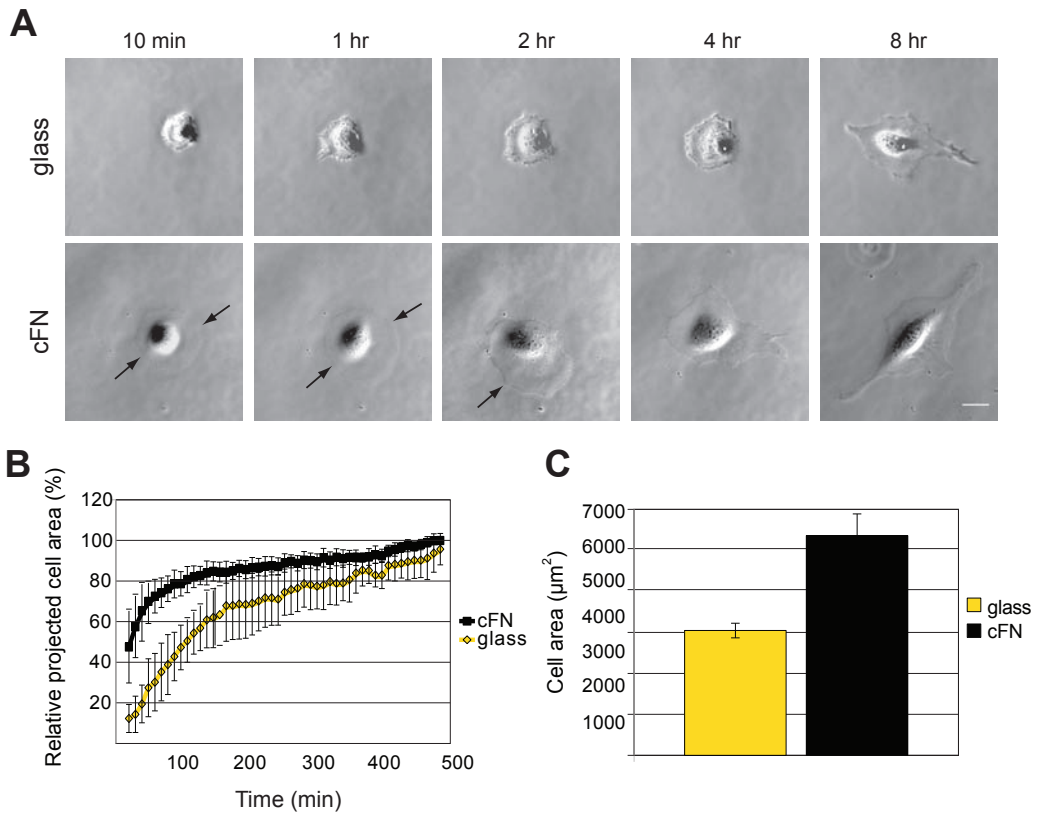

Figure 5.8: **Cell spreading kinetics of REFYFPpax cells on glass and cFN coating.** **A.** Phase contrast images show representative cells adhering on glass and cFN. Black arrows point at cell boundaries. (scale bar: 20 μm) **B.** Graph showing progression of cell area relative to the maximal cell area. **C.** Bars showing mean cell area on the two substrates.

In order to verify if REF cells stably expressing YFP-tagged paxillin (REF-YFPpax) spread with similar kinetics on FN coatings as REF52WT cells, the progression of the projected cell area was monitored on glass and on cFN (figure 5.8). Also here it was observed that cFN promoted the initial spreading and increased the mean cell area compared to untreated glass.

5.3 Molecular mechanism of fibroblast adhesion on FN coatings

5.3.1 Reorganization of pFN coatings by fibroblasts

REFYFPpax were seeded on FNs prelabeled with AlexaFluor 555 (cFN_{555}, pFN_{555}) to analyze whether fibroblasts modify the underlying coating. While cFN_{555} coatings remained intact, pFN_{555} was partially uptaken from the surface and reorganized into fibrils. Figure 5.9 shows cells adhering to a cFN_{555} coating for 20 hr. Images were acquired for 4 hr, but no significant changes in paxillin structures or in the underlying coating were observed. The fluorescence intensity of cFN_{555} was slightly lower underneath the cell periphery.

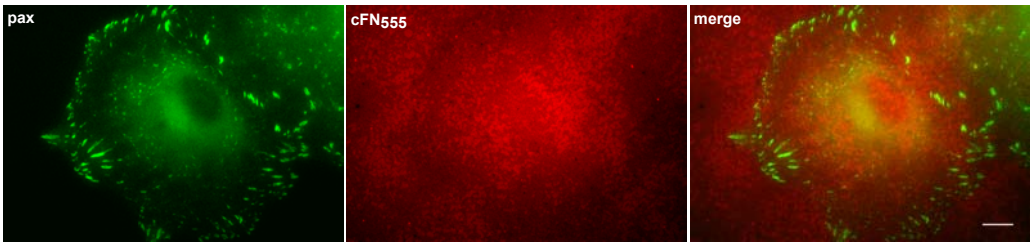

Figure 5.9: **REFYFPpax on cFN_{555}.** REFYFPpax (paxillin, green) were seeded on glass substrates coated with cFN_{555} (red). The images shown were acquired 20 hr after seeding (scale bar: 10 μm).

The left images in figure 5.10 show a REFYFPpax cell (green) on pFN_{555} (red) 20 hr after seeding. The cell shown presented focal complexes (FCs, yellow arrow), focal adhesions (FAs, white arrow) and fibrillar adhesions (FBs, blue arrow). The images in the right column show magnifications of the ROI indicated on the merged image on the left at the indicated time points.
Paxillin-rich FCs and FAs (yellow and white arrows) show an intact pFN coating underneath the cell. A partial colocalization of paxillin and fibrillar FN could be observed at some FBs (blue arrow, 7.5 min), while others only contained FN (blue arrows, 22.5 min). Pink arrows (15 min) point at spots on the surface lacking FN. In some areas, FN accumulated at the centripetal edge of paxillin clusters (gray arrows, 30 min) showing that fibroblasts were

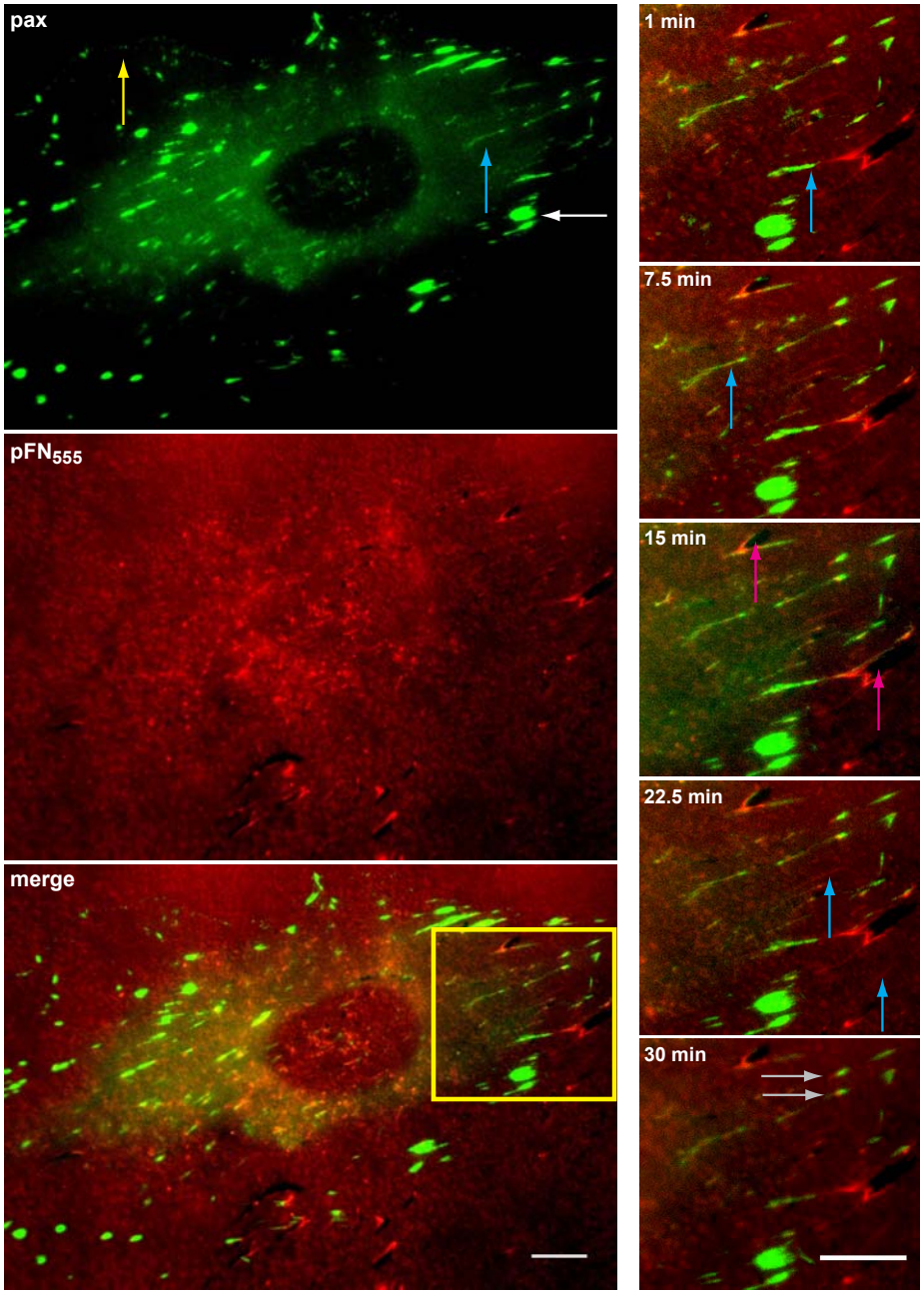

Figure 5.10: **REFYFPpax cell on pFN$_{555}$.** Arrows point at focal complexes (FCs, yellow), focal adhesions (FAs, white) and fibrillar adhesions (FBs, blue). Gray arrows indicate FN accumulation at the edge of paxillin (green) clusters and pink arrows point at spots where FN (red) has been completely removed from the substrate. The yellow box frames the ROI magnified in the right column after time points indicated. (scale bar: 10 μm)

able to partially reassemble the underlying protein coating.

5.3.2 Molecular composition and distribution of adhesion sites on different FN types

To determine if the assembly of adhesion sites was affected by the inclusion of EDA in FN coatings, the distribution of FA molecules in fibroblasts adhering to uncoated glass, cFN and pFN was analyzed by immunostaining. Fluorescence microscopy images of REFYFPpax cells stained for actin (red), paxillin (green) and vinculin (blue) are presented in figure 5.11. Paxillin and

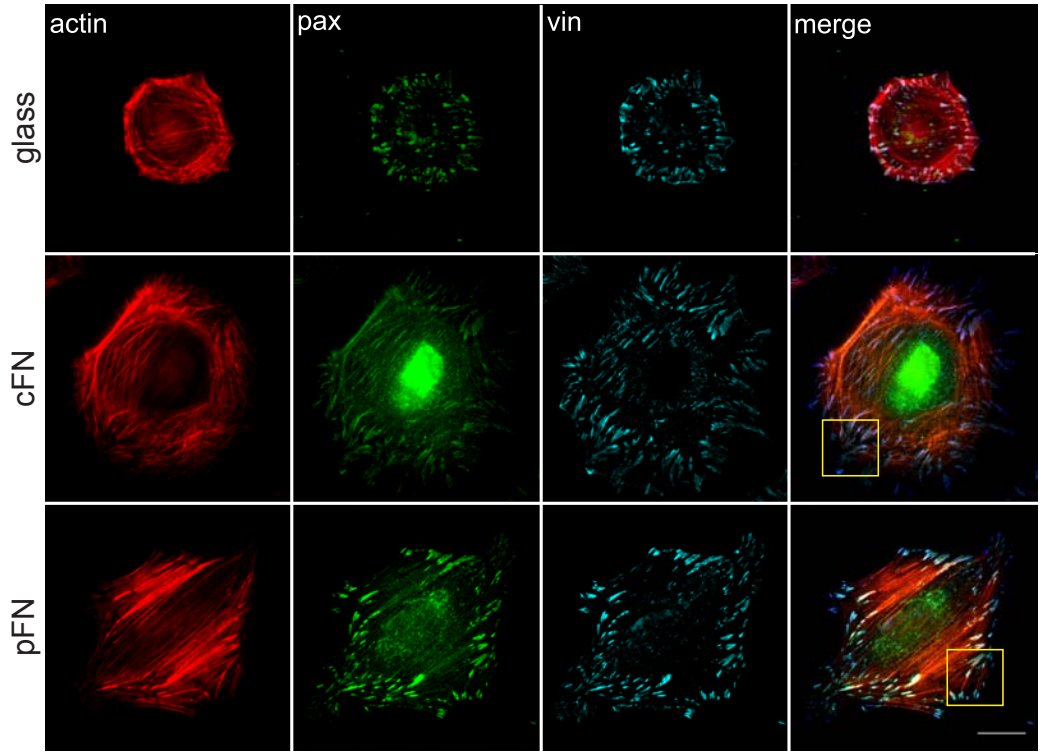

Figure 5.11: **Molecular composition of adhesion sites on FNs.** REFYFPpax (paxillin, green) cells were stained for actin (red) and vinculin (cyan) 4 hr after seeding on glass, cFN or pFN. Yellow boxes are magnified in figure 5.12. (scale bar: 20 μm)

vinculin colocalized on all surfaces; however, while they were found over the whole cell area in fibroblasts adhering to cFN, cells adhering to pFN presented a dominant distribution of adhesive structures at the cell periphery.

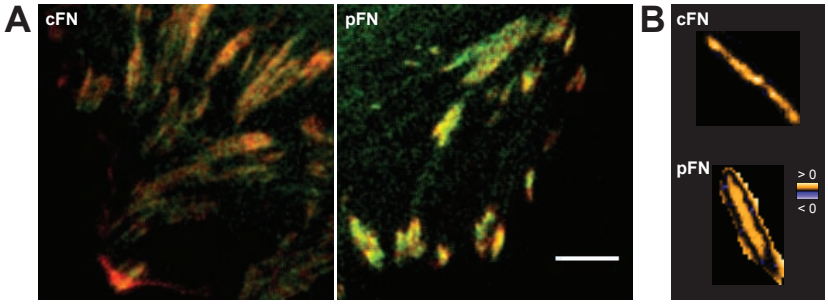

Figure 5.12: **Molecular composition of adhesion sites on FNs. A.** ROIs are indicated in figure 5.11. (scale bar: 5 μm) **B.** PDM images of two typical adhesion sites showing colocalization of paxillin and vinculin.

The organization of the actin cytoskeleton differed in that stress fibers were more pronounced and parallel to the direction of spreading in cells adhering to pFN, whereas cells on cFN presented a network of thinner fibers mostly localized along the cell perimeter. Single adhesion clusters in cells adhering to cFN had a different shape when compared to cells adhering to pFN. In these cells, paxillin clusters were elongated and radially distributed towards the cell center, whereas the contacts of cells adhering to pFN were thicker and less elongated and were localized at the cell periphery. Figure 5.12 A shows magnifications of the inserts indicated in figure 5.11. Figure 5.12 B shows two representative adhesion sites on each FN coating after processing with the intensity correlation analysis plugin from ImageJ. Here the product of the difference between the mean intensity within an image and the intensity of each pixel (PDM value) is calculated resulting in negative values, which represent a low correlation and positive values depict a high correlation. On both substrates, PDM values for paxillin and vinculin channels were positive, showing that both molecules colocalized independently from the molecular composition of the FN used for coating.

5.3.3 Zyxin-rich structures were more prominent on pFN coatings

In order to analyze the localization of zyxin, fibroblasts were transiently double transfected for YFP-paxillin and mCherry zyxin (figure 5.13). Zyxin colocalized with paxillin in peripheral structures on both types of FN and,

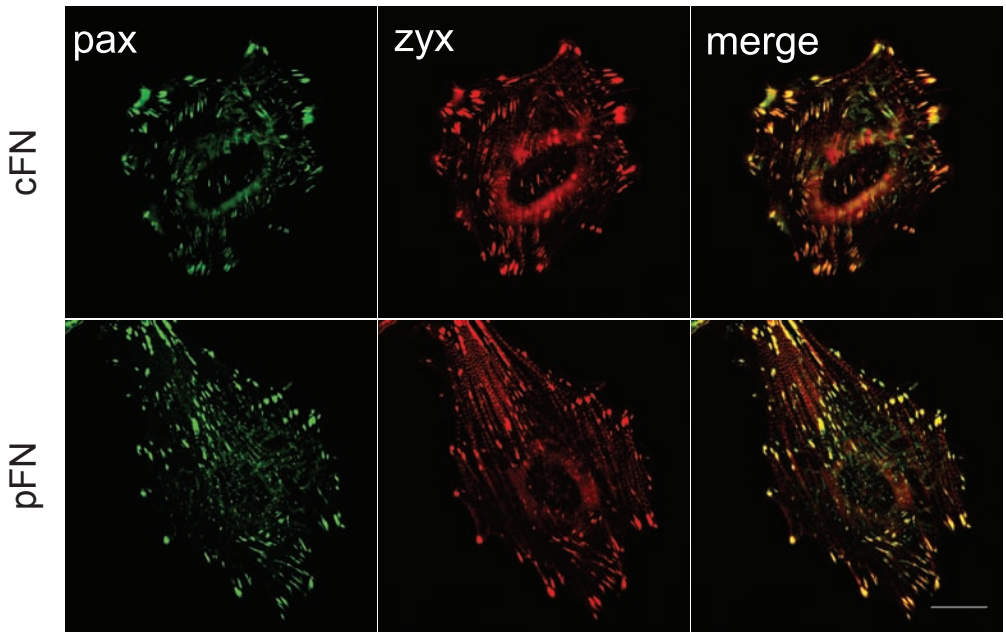

Figure 5.13: **Paxillin and zyxin distribution on FN coatings.** REF52WT were double-transfected for YFP-paxillin (green) and mCherry-zyxin (red). (scale bar: 20 μm)

in contrast to cFN surfaces, it was found along stress fibers on pFN.

5.3.4 Paxillin phosphorylation at the peripheral end of paxillin structures

Since paxillin phosphorylation at tyrosine 118 (ppax^{118}) regulates the transition from FAs to FBs, its distribution on FN coatings was analyzed by fluorescence microscopy. REFYFPpax cells were fixed and permeabilized 4 hr after seeding and stained for actin and ppax^{118} (figure 5.14).

Phosphorylated paxillin was detected mainly at the cell boundary at the peripheral edges of paxillin structures, regardless of the type of FN coating.

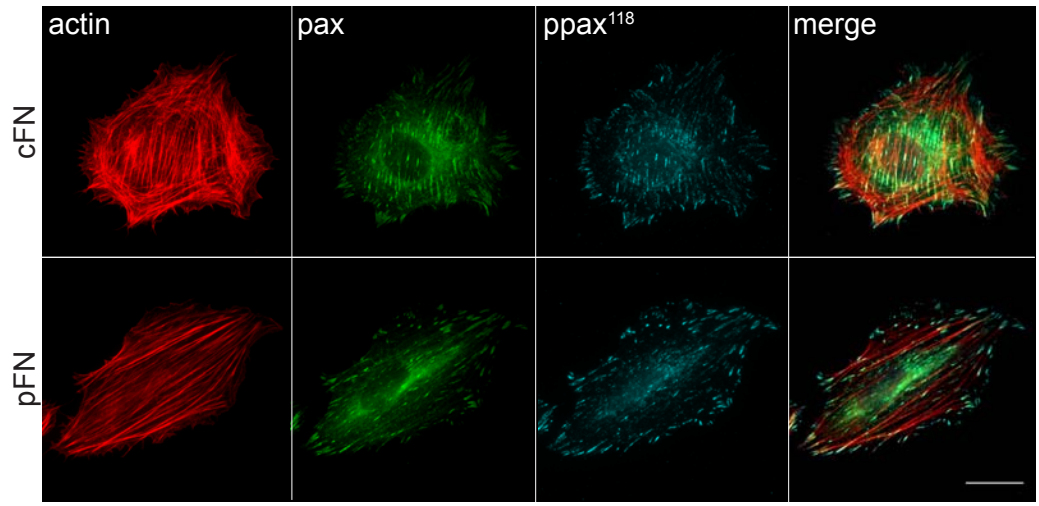

Figure 5.14: **Distribution of phosphorylated paxillin.** REFYFPpax (paxillin, green) cells were stained for actin (cyan) and phospho-paxillin at Tyr118 (red) 4 hr after seeding on cFN or pFN. (scale bar: 20 μm)

5.3.5 Distribution and shape of α_5-integrin clusters on different FN types

REF52WT cells were transfected with GFP-α_5-integrin. One day after the transfection, cells were seeded on cFN or pFN coatings and imaged 24 hr after plating. α_5-integrin structures on the two substrates differed in both

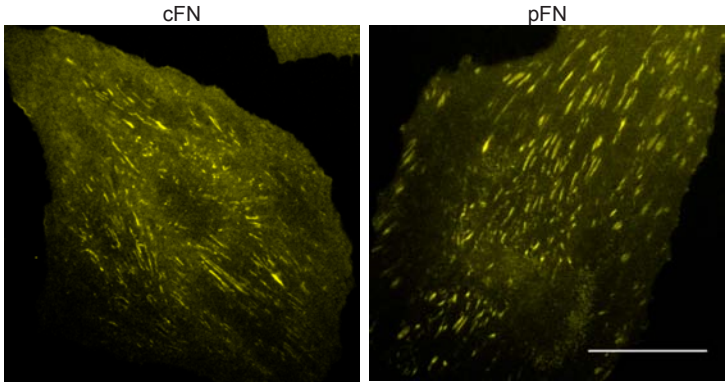

Figure 5.15: **REF52WT on physisorbed FNs.** Cells transfected with GFP-α_5-integrin were seeded on cFN and pFN. The images were acquired 24 hr after seeding. (scale bar: 20 μm)

distribution and shape. While thinner and longer structures located mainly at central parts of the cell on cFN, integrin clusters on pFN appeared thicker and shorter on pFN coatings, where they were also found at peripheral sites of cells.

5.3.6 The mode of FN adsorption affected the distribution of α_5- and β_3–integrin

To investigate if the mode of FN adsorption affected the distribution of integrins, cells were seeded either on directly or indirectly physisorbed FNs and immunostained for β_3- (green) and α_5-integrins (red).
Since the available antibodies were not specific for rat cells, human CDP (cells of the dental pulp), another type of mesenchymal cells, were used.
Figure 5.16 shows the typical distribution of these integrins in CDP cells. Thin, elongated structures were found in cells seeded on cFN, compared to pFN coated substrates, where clusters appeared thicker but also shorter. While these structures localized over the whole cell surface on directly physisorbed cFN, they were predominantly found at the periphery of cells seeded on pFN and on indirectly physisorbed FNs.
In order to investigate the impact of distinct FN types and modes of adsorption on the localization of integrins, CDP cells were seeded on the different coatings and stained for integrins (figure 5.16).

5.3.7 The mode of adsorption of FN did not affect paxillin phosphorylation at Tyr118

Since the phosphorylation state of paxillin at tyrosine 118 plays a crucial role in the regulation of focal and fibrillar adhesion formation, the phosphorylation of paxillin at this site was characterized with western blotting.

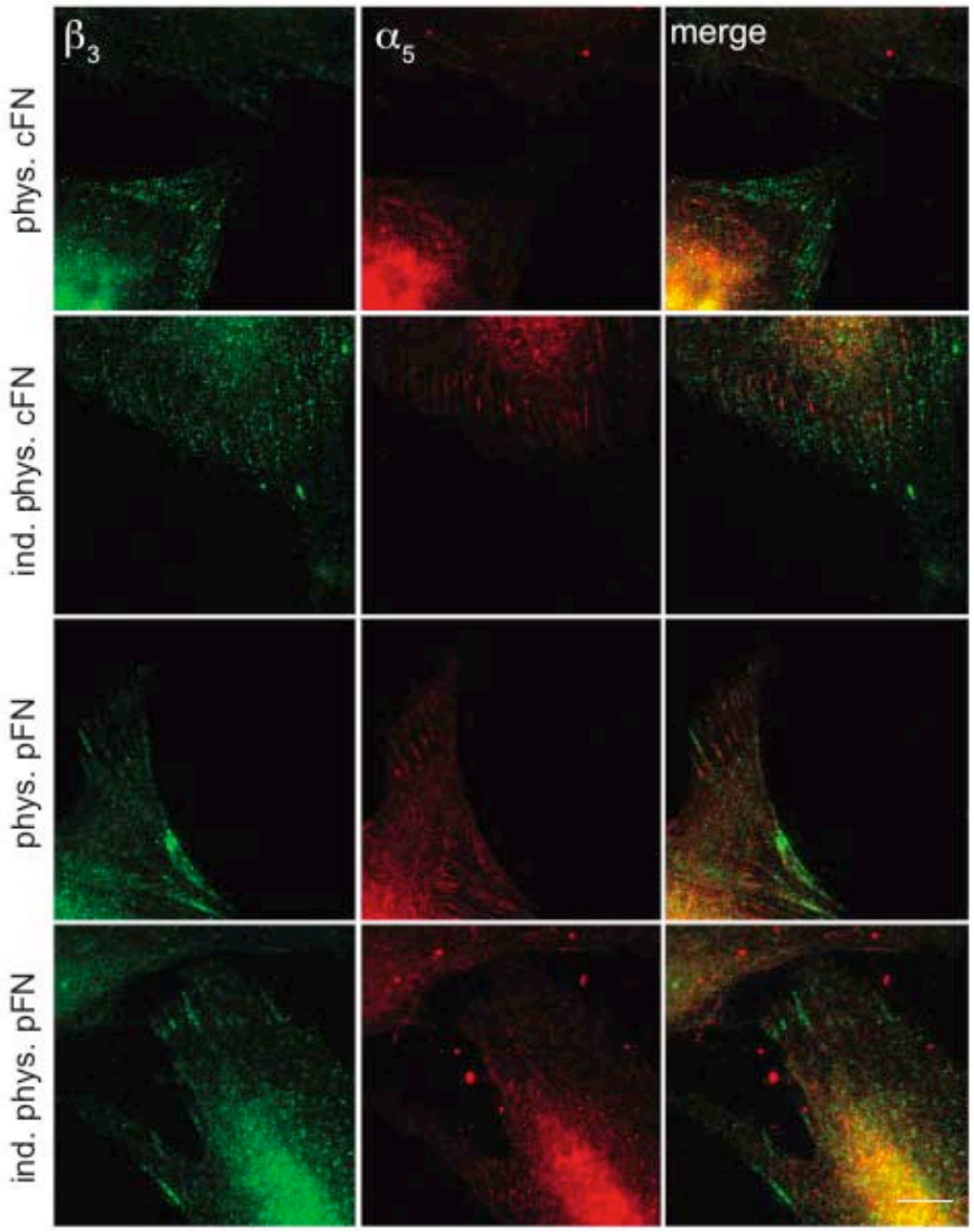

Figure 5.16: **CDP integrin staining on directly and indirectly physisorbed FNs.** β_3-integrins are shown in green, α_5-integrins in red. (scale bar: 10 μm)

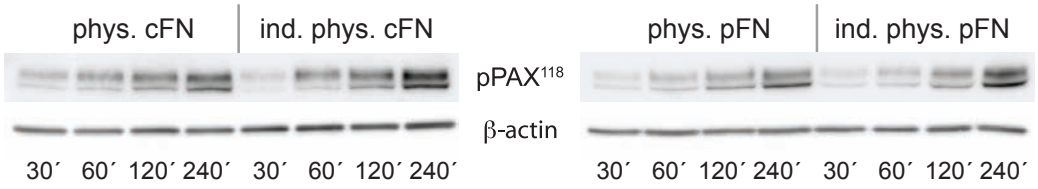

Figure 5.17: **Western blotting of REF52WT cell lysates.** The expression of pPAX^{118} on directly and indirectly physisorbed FNs was tested after the indicated time points.

Therefore, protein extracts of REF52WT adhering for 30, 60, 120 and 240 min on the substrates were analyzed. Figure 5.17 shows characteristic double bands for pPAX^{118} at 66 kDa. β-actin was used as loading control. On all four substrates paxillin phosphorylation increased linearly with time. The intensity of the bands was compared and no differences were observed regardless of the mode of adsorption.

5.4 FN fibrillogenesis on FN coatings and FN-derived peptides

5.4.1 Role of FN for fibroblast adhesion on cRGDfK

MEF $FN^{-/-}$ cells (for description and reference see 4.4.1) failed to adhere to nanopatterns functionalized with cyclic RGD (RGD-NPs) when cultured and seeded in serum-free media. Even when 1% FCS was added to the media after seeding on the substrates, the knockout cells did not adhere, regardless of the inter-ligand distance ranging from 30 to 110 nm, whereas control MEF $FN^{fl/fl}$ adhered on all NPs. Figure 5.18 shows an example of the two cell types seeded on nanopatterned surfaces presenting an inter-ligand distance of 30 nm. Adhesion and survival of $FN^{-/-}$ cells on RGD was only observed when they were cultured in DMEM supplemented with 10% FCS, suggesting that the presence of either endogenous or exogenous serum FN, in combination with growth factors present in serum, is required for fibroblast survival and adhesion on cRGD.

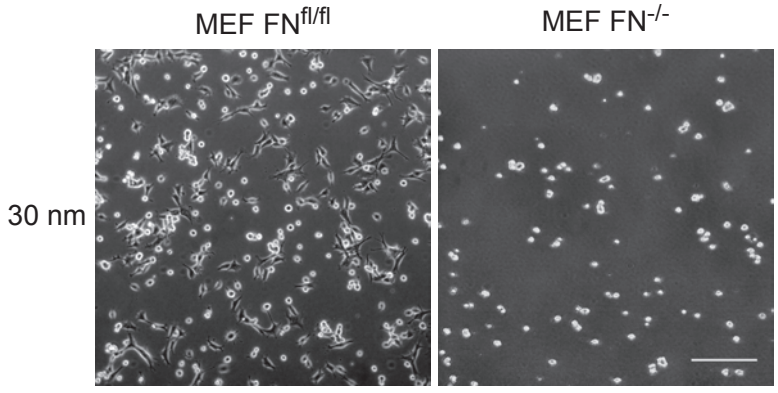

Figure 5.18: **MEF $FN^{-/-}$ cells failed to adhere on RGD-functionalized substrates.** MEF $FN^{fl/fl}$ adhered and spread on nanopatterned surfaces presenting an inter-ligand spacing of 30 nm, while MEF $FN^{-/-}$ failed to attach. (scale bar: 100 μm)

5.4.2 Fibroblasts secreted and deposited FN on the substrate and assembled it into fibrils

In order to analyze the localization of the secreted FN, REFYFPpax fibroblasts were imaged using total internal fluorescence (TIRF) microscopy (see 4.6.2), which allows to selectively visualize the plane on the plasma membrane. Fig 5.19 shows that exogenous FN was assembled into fibrils that were co-aligned with paxillin clusters. Indeed, these images show that FN was deposited at the ventral side of the cells, where also paxillin structures were formed.

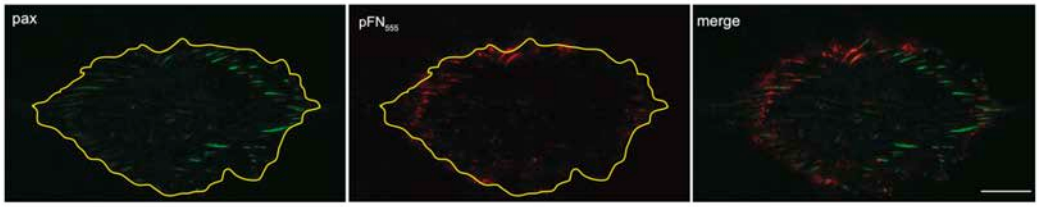

Figure 5.19: **Exogenous FN is assembled and deposited on the substrate** REFYFPpax cell on cFN 4 hr after seeding and 1 hr after the addition of pFN_{555}. (scale bar: 20 μm)

5.4.3 The distinct FN types differentially regulated the distribution and assembly of FN fibrils

To determine the effects of pFN and cFN coatings on the formation of *de-novo* contacts and the assembly of FN fibrils, pFN_{555} was added to cell culture media and cells were observed for 4 hr with fluorescence microscopy. Figure 5.20 shows ROIs of two REF52WT transfected with GFP-α_5-integrin adhering to directly physisorbed cFN and pFN. In both conditions it was observed that the pFN_{555} added to the media was partially assembled into fibrils by cells as α_5-integrins translocated towards the cell center. Fibrillar integrin structures colocalized with FN and correlated with the length and number of FN fibers. While more fibrillar integrin and FN structures were seen on cFN, less and shorter fibrils were found on the cell periphery of fibroblasts grown on pFN. The FN fibril length was quantified with ImageJ

by measuring selected ROIs. It was observed that the average length was higher on cFN (ranging from 0.61 to 28.80 μm) in comparison to the length on pFN (0.15 to 8.29 μm). These results showed that the distinct types of FN affect both α_5-integrin distribution and organization of soluble FN differentially.

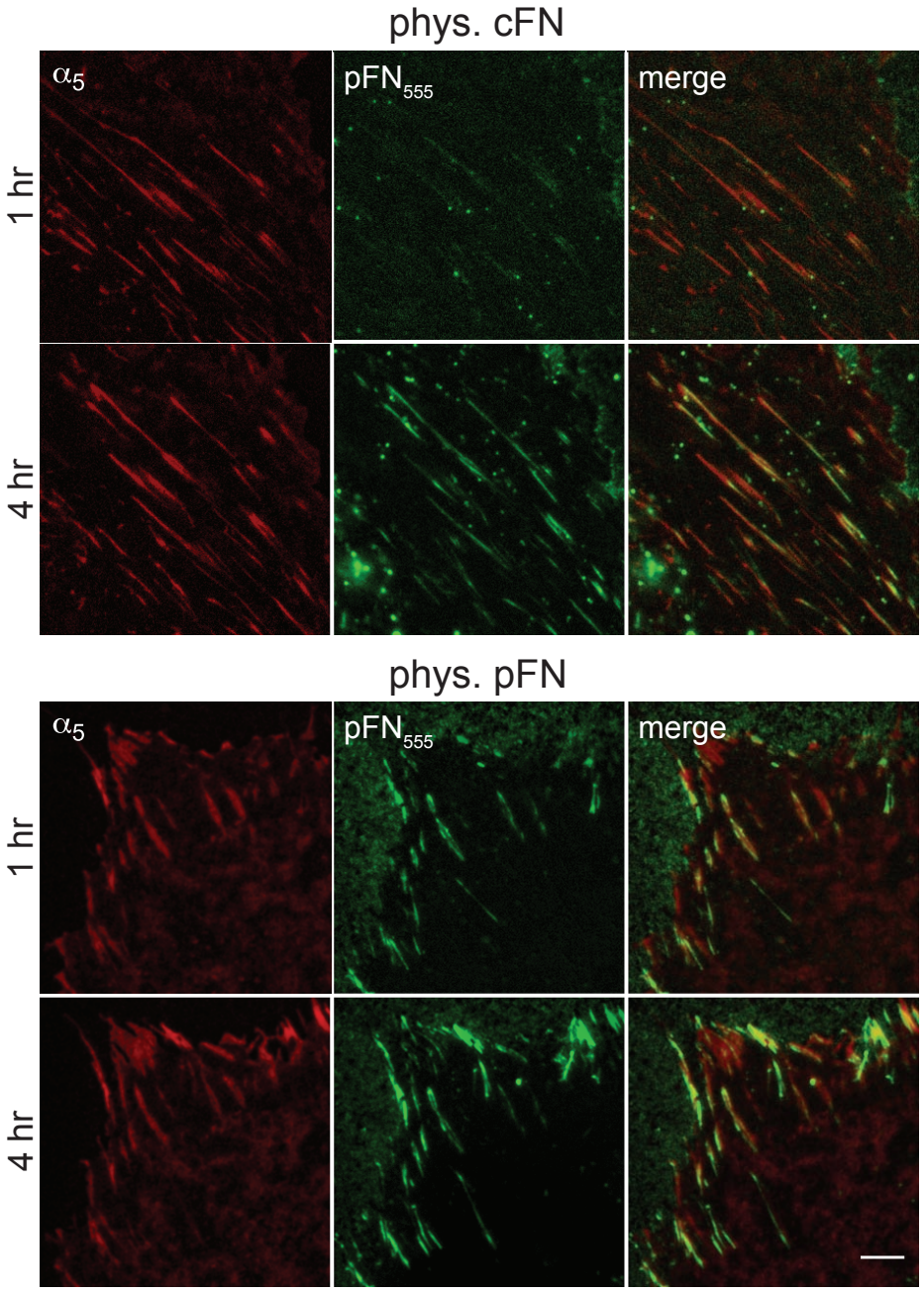

Figure 5.20: **Assembly of exogenous fibronectin.** REF52WT cells were transfected with GFP-α_5-integrin (red). Prelabeled pFN (green) was added to the media and changes in integrin and FN distribution were monitored for the first 4 hr after the addition of FN. (scale bar: 5 μm)

5.4.4 cFN promoted the formation of elongated α_5-integrin clusters and their centripetal translocation

REF52WT cells were transfected with GFP-α_5-integrin and seeded on cFN or pFN coatings. 16 hr after adhesion, 10 μg/ml of pFN_{555} was added to the media and changes in integrin distribution and FN organization were monitored during the first 4 hr after the addition of exogenous FN. In both conditions α_5-integrins translocated towards the cell center.

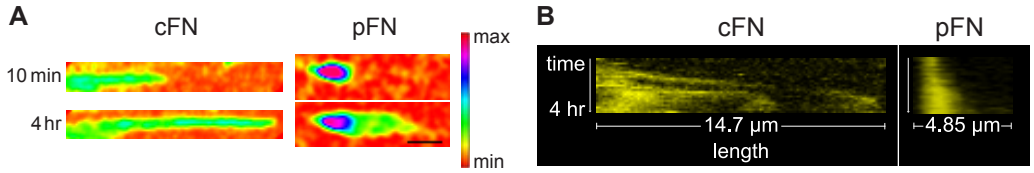

Figure 5.21: **α_5-integrin cluster formation and translocation on cFN and pFN. A.** Fluorescence intensity distribution within two typical α_5-integrin clusters 10 min and 4 hr after addition of prelabeled pFN. (scale bar: 2 μm) **B.** Kymographs of α_5-integrins after the addition of exogenous FN.

The intensity distribution of two typical clusters is shown in figure 5.21 A in a spectrum scale as indicated in the lookup table. The intensity distribution was homogeneous within growing structures on cFN. This was in clear contrast to structures observed on pFN, where it remained higher at the cell periphery. The velocity of growth of integrin clusters was quantified using kymographs (figure 5.21 B). A faster centripetal translocation of α_5-integrin was observed in cells adhering to cFN in comparison to cells adhering to pFN, with an average value of 2.10 ± 0.90 μm/hr for cFN and 1.08 ± 0.80 μm/hr on pFN, indicating that EDA-containing cFN promoted a faster FB formation.

5.4.5 The inter-ligand spacing of cRGDfK peptides affected actin organization and FN assembly

REF52WT were seeded on nanopatterned substrates functionalized with cRGDfK peptides (as described in section 4.2) and fixed after 4 or 24 hr for staining of actin stress fibers and endogenous FN (figure 5.22). Homoge-

neous gold surfaces with immobilized cRGDfK (hRGD) were used as control. 4 hr after plating on hRGD and on 58 nm patterns fibroblasts presented a similar circular shape, but the cell area was higher on hRGD. On these two substrates actin formed concentric ring-like structures. On nanopatterned substrates with higher inter-particle distances (73 and 110 nm) cell adhesion was reduced. Furthermore, no organization of actin stress fibers was visible.

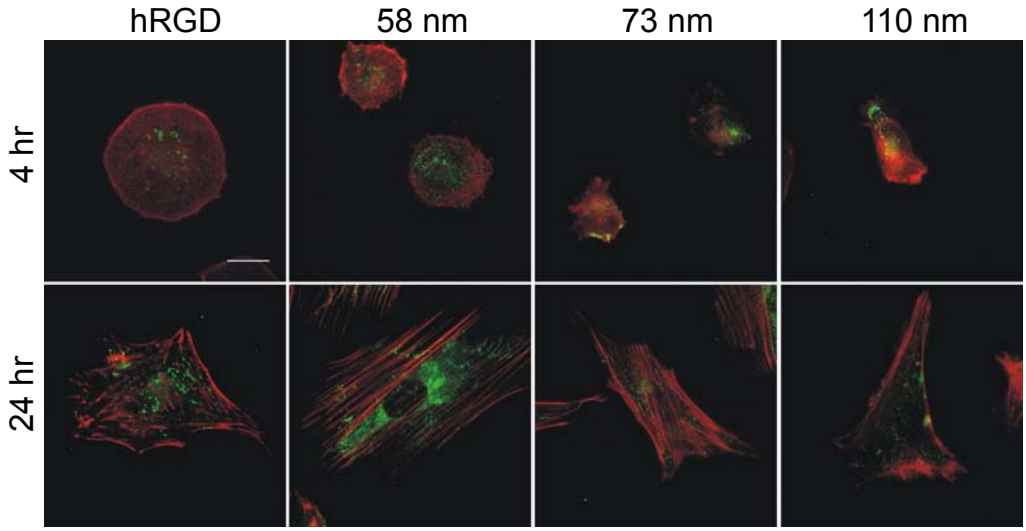

Figure 5.22: **Single fibroblasts on RGD-NPs.** REF52WT were stained for actin (red) and endogenous FN (green) 4 and 24 hr after seeding on nanopatterned substrates presenting cRGDfK. The inter-ligand spacing is indicated above.(scale bar: 20 μm)

FN accumulations were observed on all substrates already 4 hr after seeding. Only on 58 nm patterns, short FN fibrils distributed radially over central parts of the cell.

After 24 hr cells were spread on all substrates, but showed differences in shape, stress fiber formation and FN organization. On hRGD and on nanopatterns presenting an interparticle distance of 73 or 110 nm, fibroblasts failed to form actin stress fibers, in contrast to cells adhering to 58 nm patterns. Here, stress fibers were organized parallel to the major axis of cells. These results showed for the first time that the distance between neighbouring ligands had an effect not only on cell shape and actin organization, but also on the assembly of FN.

5.4.6 Effect of cell density on FN fibrillogenesis

FN fibrils were observed on gold nanopatterned substrates regardless of the inter-particle distance when cells were seeded at a higher density. Fibrils were observed over the whole cell area on hRGD substrates and to a greater extent on 58 nm, where they appeared thicker and denser. On substrates where the distance between neighbouring peptides was higher, globular FN was found at central parts of fibroblasts, but on all substrates the major part of the protein was detected at cell-cell contacts, where it was organized into fibrils (figure 5.23).

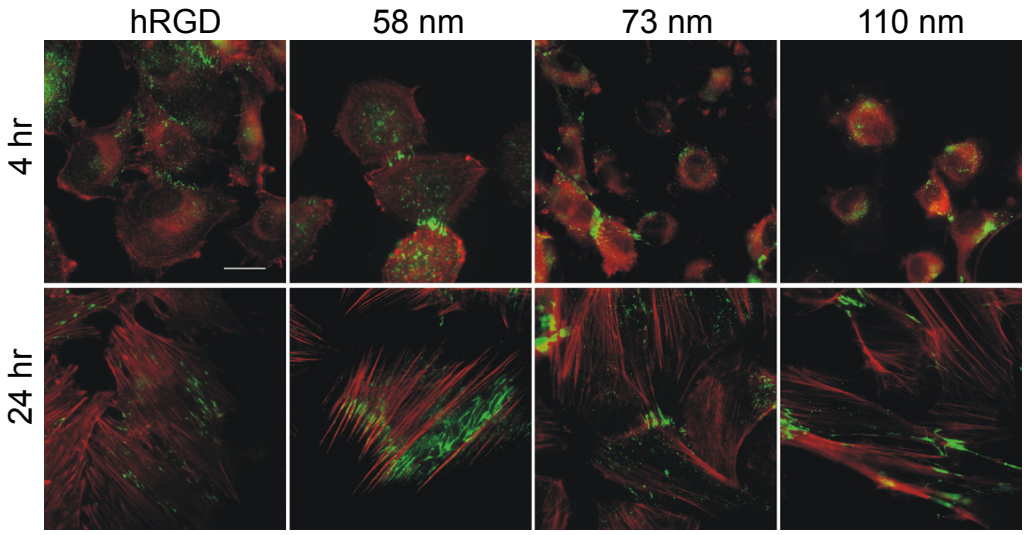

Figure 5.23: **FN organization at cell-cell contacts.** REF52WT were seeded on nanopatterned substrates presenting cRGDfK and stained for actin (red) and endogenous FN (green). Note FN accumulation and fibril formation at cell-cell contacts on all substrates (scale bar: 20 μm).

5.4.7 The synergy site PHSRN enhanced cell adhesion and FN assembly

3T3YPet-FN cells were seeded on gold nanopatterned substrates functionalized with either cRGD or $FNIII_{9-10}$. 4 hr after seeding, cells showed a rather circular shape on cRGD, in contrast to $FNIII_{9-10}$, where they presented a

more flattened and elongated shape and a larger area (figure 5.24). In order

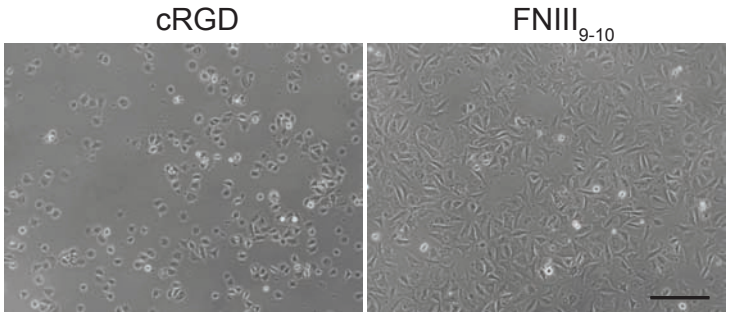

Figure 5.24: **Fibroblasts adhering on cRGD or FNIII$_{9-10}$ for 4 hr.** 3T3YPet-FN cells were seeded on nanopatterned glass substrates functionalized with either cRGD or FNIII$_{9-10}$ (scale bar: 100 μm).

to analyze the formation of adhesion sites on the different ligands, cells were fixed and permeabilized for immunostaining. Figure 5.25 shows that FAs

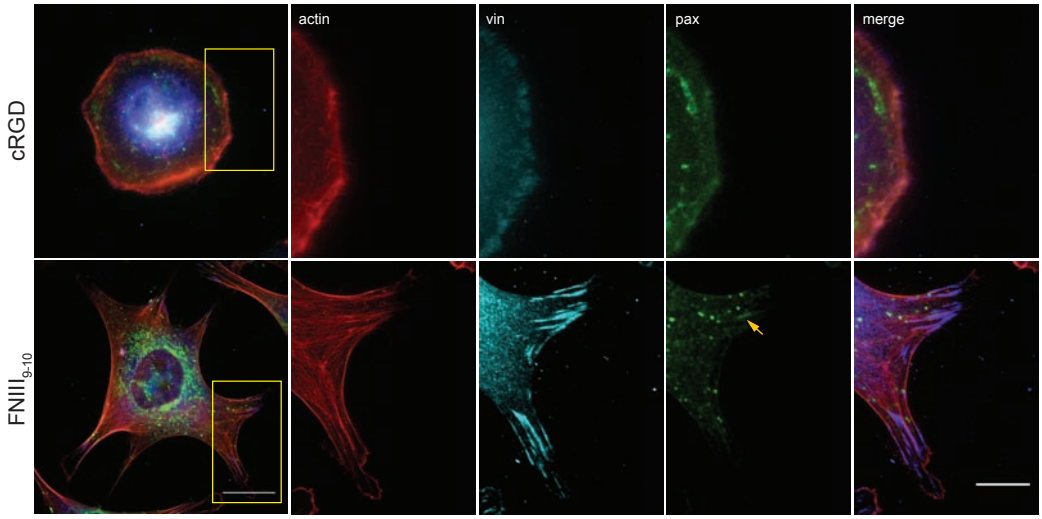

Figure 5.25: **Staining of adhering 3T3YPet-FN cells on cRGD or FNIII$_{9-10}$ for 4 hr.** Two cells adhering on the different samples are shown in the left column (scale bar: 20 μm). The yellow boxes indicate the inserts magnified on the right. Actin is shown in red, vinculin in cyan and endogenous FN in green. The arrowhead points at a FN fibril. (scale bar: 10 μm).

formed after 4 hr only on the fragment containing the cell binding domain and its synergy site in FNIII$_{10}$. Moreover, a few FN fibrils were detected

on these samples, while FN was only found as dot-shaped accumulations on cRGD.

6 Discussion

Fibronectins mediate cell adhesion to the extracellular matrix (ECM) and are therefore widely used as adhesive substrate for *in vitro* studies of adherent cells [Yamada and Olden, 1978]. Although cFN is the type of the protein that is deposited locally and assembled into an insoluble matrix to promote cell adhesion *in vivo*, it is not commonly used as an adhesive coating. Instead, pFN is the protein of choice, due to its lower cost and higher availability. Although both FN types are derived from the same gene, they differ in their molecular composition as a result of alternative splicing [Kornblihtt et al., 1996]. The effects of extra domains that are exclusively present in cFN on cell adhesion are controversial [Manabe et al., 1997, Guan et al., 1990]. The aim of this work was to determine how pFN, cFN and FN-derived peptides regulate the formation of adhesive contacts and FN assembly.

Cell adhesion not only occurs between cells and the ECM but also between adjacent cells. Since the objective of this study was the investigation of cell-substrate interactions, only cells that were not in contact with each other were analyzed.

The focus lied on the segregation of focal (FA) into fibrillar adhesions (FB), a critical step in the process of FN assembly. Therefore, the distribution of FA proteins, such as paxillin - a key regulator of FN signaling - were characterized in fibroblasts, which in turn produce and assemble cellular FN. Special emphasis was placed on FN fibrillogenesis due to its impact on ECM assembly. Since α_5-integrins are known to translocate from FAs to FBs stretching FN to allow its polymerization, the localization and dynamics of α_5-integrin clusters were monitored.

6.1 FN coatings on glass surfaces

QCM-D was used to analyze the time-dependency and mass of protein deposition on silicon oxide. The measurements showed that FNs adsorb within the first 60 min after incubation, regardless of the type of FN used. These results are in agreement with a previous study on pFN adsorption on silicon oxide surfaces [Al-Jawad et al., 2009]. The amount of adsorbed protein was also in the same range. In the present work, the deposition of pFN and cFN was measured for the first time and yielded a higher adsorbed mass for the second type of the protein. The amount of protein could not be calculated in molar concentration, due to the different lengths of the dimers that arise from alternative splicing. The protein structure of cFN could favor the exposure of hydrophilic aminoacids, enhancing interactions with the hydrophilic surface. Nevertheless, QCM-D measurements had to be repeated several times due to high variances in frequency changes in the different repeats. These inconsistencies could be associated with the high sensitivity of the device, e. g. nano-bubbles introduced into the liquid chamber interfere with the measurements. In terms of time-dependency, though, both FN types behaved similarly throughout all the experiments.
BSA was used to block the uncoated glass surface in order to prevent unspecific cell binding. QCM-D measurements showed a decrease in the frequency as 1% BSA solution was pumped into the chambers. The protein could either adsorb on the glass or on the preadsorbed FNs.
When DMEM supplemented with FBS was added to the precoated crystals, frequency levels decreased, showing that serum components adsorbed on the coatings. Since some of the serum components could influence cell adhesion and target membrane proteins other than FN receptors, it was necessary to analyze the protein contents of FBS used for cell experiments (see 6.2).

6.2 Role of serum proteins in cell adhesion

The composition of serum is usually not characterized by companies nor users. Since some of its protein contents could promote cell adhesion, FBS

and purified FN solutions were analyzed by SDS-PAGE and subsequent Coomassie staining or western blotting.
The major ligand for $\alpha_v\beta_3$-integrins is the cell-adhesive protein vitronectin [Akiyama et al., 1990]. Therefore, its absence in the FN preparations and in serum was tested. The differences in the formation of adhesion sites on the coatings can therefore not be attributed to this potential contaminant. It is known that high concentrations of serum can affect cell adhesion. For

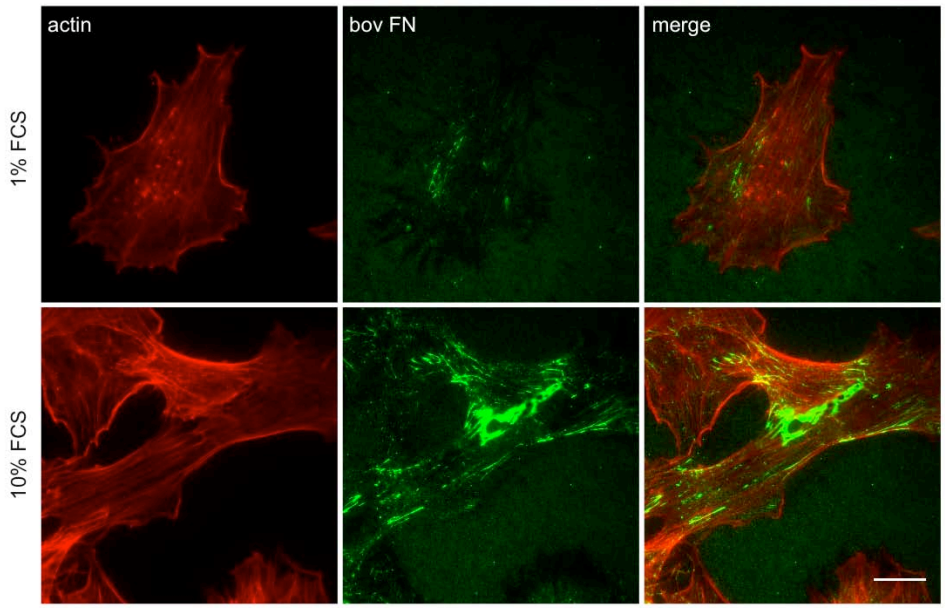

Figure 6.1: **Fibroblasts assemble serum FN into fibrils.** NIH3T3 cells on glass substrates fixed and stained for actin (red) and bovine FN (green) 4 hr after seeding (scale bar: 20 μm).

this reason, cell experiments were performed with a controlled serum concentration. In order to exclude the presence of serum proteins to ensure that adhesion was promoted only by the provided substrate coating, cells were serum deprived before seeding.
Figure 6.1, shows NIH3T3 cells adhering on uncoated glass grown in DMEM containing two different concentrations of FCS. Serum FN not only deposits on glass, but it can also be assembled into fibrils by fibroblasts.
Since an increase in the serum concentration yields higher FN fibrillogenesis and cell adhesion is inhibited in the absence of serum, a concentration of 1 %

FBS or FCS was used in all cell experiments.

6.3 Role of EDA in cell adhesion

Several isoforms of FN arise from alternative splicing at the domains EDA, EDB and IIICS. While IIICS is present both in cFN and pFN, the extra domains EDA and EDB are only included in cFN [Kornblihtt et al., 1985]. It has been observed that the EDA domain, in contrast to EDB, has an effect on cell adhesion. It has been reported that recombinant EDA-containing FN was more potent than FN lacking the EDA sequence in inducing spreading of fibrosarcoma cells [Manabe et al., 1997]. cFN showed the same tendency when compared to pFN, although the differences were not as striking as in the first case. A similar effect was observed in synovial cells [Hino et al., 1996]. In other cell types, such as baby hamster kidney cells (BHK), however, no differences were detected [Yamada and Kennedy, 1979]. These seemingly contradictory observations can be attributed to a cell-dependent integrin expression.

The EDA-sequence was shown to induce a conformational change within the FN molecule, thus increasing the affinity for $\alpha_5\beta_1$-integrin. EDA was also identified as a ligand for other integrin types. One of them is $\alpha_9\beta_1$, which is constitutively expressed in rat keratinocytes and mediates cell adhesion to EDA [Shinde et al., 2008]. EDA was also reported to promote $\alpha_4\beta_1$ [Liao et al., 2002] and $\alpha_4\beta_7$ [Kohan et al., 2010] mediated adhesion and to affect cell signaling. The presence of EDA was assessed in cFN used in this study. Fibroblasts were tested for cell spreading kinetics on the two types of the protein and on glass. In agreement with previous studies, both FNs promoted cell adhesion when compared to untreated glass. A comparison between the two FNs showed no significant differences in the spreading nor in the projected cell area, showing that EDA is dispensable for cell spreading in fibroblasts.

6.4 Molecular composition of FAs on different FNs

Cells sense their environment through different membrane receptors that can mediate adhesion. Different types of adhesion sites were identified in cells cultured on rigid, flat surfaces.
The distribution of various adhesion site markers was analyzed on the two FN types. FAs were found 4 hr after seeding on the coatings and were rich in paxillin and vinculin. These two proteins strongly colocalized on the two coatings. However, slight differences were observed regarding the localization and shape of adhesion sites, which were found over the entire surface of cells seeded on cFN. While the majority of these structures in cells adhering to pFN located predominantly at the cell periphery, they presented a more elongated shape in fibroblasts seeded on cFN coatings.

6.5 Effect of immobilization of cell-adhesive ligands on adhesion

To investigate how the mode of deposition of the coating affects the formation of adhesive contacts, the two types of FN were either directly physisorbed on glass or cross-linked on an subjacent layer of poly-L-lysine according to Katz et al. [Katz et al., 2000]. Furthermore, discrete FN fragments or FN-derived peptides were immobilized on nanopatterned surfaces in order to analyze how they regulate cell adhesion and FN assembly. Substrate nanopatterning and functionalization with specific ligands were employed, since they allow the regulation of integrin activation and lateral clustering [Arnold et al., 2004, Cavalcanti-Adam et al., 2007]. Thus, this technique is useful to control the formation of FAs [Cluzel et al., 2005], which are precursors of FBs [Zaidel-Bar et al., 2004, Zamir and Geiger, 2001].
In agreement with this model, it could be observed that substrates that favor the formation of stable FAs allowed the assembly of actin into stress fibers and FN fibrillogenesis. When the distance between cRGD peptides was increased, thus hindering FA formation, assembly of FN was also compromised and it was found in an inactive state.

In this work, a FN fragment including the RGD sequence and the synergy site PHSRN was immobilized on gold nanostructures for the first time. The employed technique allows control of the orientation of the protein fragment and the accessibility of the cell binding domain. When cells were seeded on these surfaces, they showed better adhesion than on cRGD, indicated by the cell size and the organization of actin and vinculin. Shortly after seeding, it could be also observed that FN fibrils were starting to form.

6.6 α_5-integrin dynamics and FN assembly

In this work it was observed that FA composition on different FNs was similar, but differences were found in dynamics of α_5-integrins and FN assembly. A possible explanation for this observation could be the distinct molecular compositions of the two types of the protein, based on the presence of the extra domain A (EDA) in cFN. It has been previously shown that this alternatively spliced domain of FN increases the affinity to $\alpha_5\beta_1$-integrins [Manabe et al., 1997], probably because EDA favors an open conformation of FN [Johnson et al., 1999].

6.7 Role of endogenous FN in cell adhesion

Fibronectin-null cells were grown in serum-free medium, allowing a control of the levels of fibronectin in the system. However, when MEF $FN^{-/-}$ were seeded on nanopatterns presenting cRGD-peptides, adhesion was abrogated. Control cells MEF $FN^{fl/fl}$, which are able to synthesize FN, in contrast, did spread and adhere on these substrates, suggesting that endogenous FN is indispensable for cell adhesion to nanopatterned surfaces. TIRF imaging revealed that FN is deposited by adhering fibroblasts on the underlying surface. These observations indicate that the presence of cRGD alone is not sufficient to mediate adhesion of MEF $FN^{-/-}$ cells and are in agreement with previous studies. It has been shown that microvascular cells cannot adhere on pFN upon blocking with an anti-FN antibody, while human umbilical vein cells (HUVEC) did [Clark et al., 1986]. This was explained by the fact that the

first type of cells, in contrast to HUVEC, is not able to synthesize endogenous FN, which could compensate for the lost adherence.

7 Conclusions and outlook

The two physiologically ocurring types of FN differ in their molecular composition and structure. Previous studies indicated that the EDA domain, which is exclusively present in cFN, has an effect on the global conformation of the protein, increasing the accessibility of RGD for $\alpha_5\beta_1$. This domain was also shown to affect cell adhesion.

In this work, it was studied how pFN and EDA-containing cFN influence cell spreading, the formation of FA and FB and FN fibrillogenesis. While both FNs yielded similar spreading kinetics, FA formation and phosphorylation of paxillin at the peripheral edge of adhesions, cFN favored the transition from FA to FB and FN assembly. This type of the protein promoted the formation of more elongated adhesions distributed over the entire cell and the translocation of α_5-integrins in centripetal direction.

It was concluded that extra domains in cFN play a role in fibroblast adhesion mediated by this type of integrin enhancing FB formation. These observations indicate that this type of the protein might contribute to the stabillity of cell-ECM interactions *in vivo*, while pFN acts mainly as an adhesive molecule by inducing the assembly of robust FAs. However, the mechanism regulating the differential effects of the distinct FN types on FB formation need to be elucidated. The differences observed could be attributed to the fact that extra domains in cFN not only represent further integrin binding sites, enhancing the translocation of the receptors, but also increase the accessibility of RGD in the central cell binding domain of the protein.

Moreover, this study offered further insights into the contribution of the lateral organization of integrin ligands on the assembly of adhesions. It has been previously shown *in vitro* that the spacing between $\alpha_v\beta_3$-integrin ligands is critical for cell adhesion. An inter-ligand spacing of 58 nm induced stable FA formation, which was inhibited at higher distances. This work showed that the spatial organization of these ligands additionally plays a role in FN fibrillogenesis. These observations are in agreement with previous studies indicating that FA formation is indispensable for FBs to arise.

Hence, FN assembly can be regulated by controlling cell adhesion through the immobilization of specific integrin ligands on surfaces. Nevertheless, the

mechanism underlying the modulation of FA and FB formation by the spatial arrangement of integrin ligands remains to be determined.

8 Appendix

8.1 Colocalization of paxillin and YFP-paxillin

24 hr after seeding on uncoated glass substrates, REF52YFP-paxillin cells were fixed and permeabilized for indirect immunostaining of paxillin. Typical images are shown in figure 8.1 **A** and **B**. The background from the

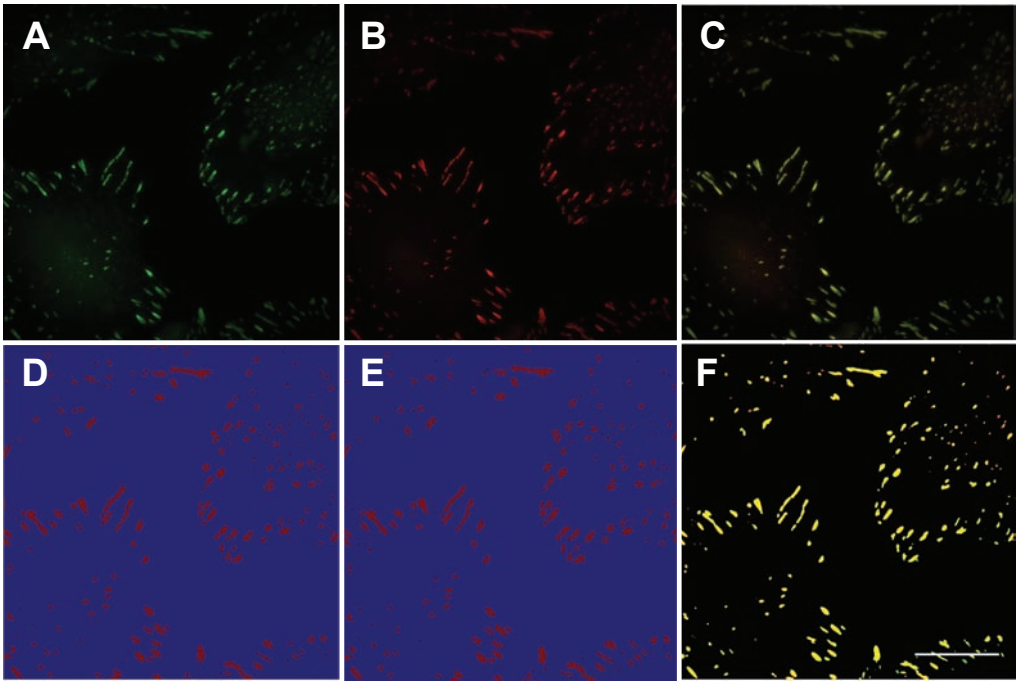

Figure 8.1: **Immunostaining of paxillin in REF52YFP-paxillin.** Cells were seeded on glass substrates, fixed and permeabilized after 24 hr for immunostaining of paxillin. **A.** YFP-tagged paxillin. **B.** Immunostained paxillin. Overlay of images A and B is shown in **C.**. Thresholded images A and B are shown in **D** and **E**, respectively. **F.** presents merged fluorescence patches in boxes D and E. Colocalized pixels are shown in yellow. (scale bar: 20 μm.)

acquired images was substracted and a threshold was applied to generate binary images (figure 8.1 **D** and **E**). Binary images of YFP-paxillin and immunostained paxillin were merged showing colocalized pixels in yellow (figure 8.1 **F**). Two colocalization coefficients were determined to characterize

the degree of overlap between the two channels. Manders coefficient was 0.91 ± 0.02 [Manders and Verbeek, 1993] and Pearson coefficient 0.9 ± 0.03, where 0 represents a random distribution of both channels and 1 indicates a perfect colocalization [Gonzalez and Wintz, 1987] .

8.2 List of abbreviations

cFN	cellular fibronectin
BCA	bicinchoninic acid
BSA	bovine serum albumin
CAPS	3-(Cyclohexylamino)-1-propanesulfonic acid
CCBD	central cell-binding domain
CDP	cells of the dental pulp
cRGDfK	cyclic Arg-Gly-Asp-Phe-Lys
DMEM	Dulbecco's modified Eagle's medium
EDTA	ethylenediaminetetraacetic acid
FA	focal adhesion
FB	fibrillar adhesion
FC	focal complex
FCS	fetal calf serum
FN	fibronectin
GFP	green fluorescent protein
MOPS	4-morpholinepropanesulfonic acid
PBS	phosphate buffered saline
PBS-T	phosphate buffered saline with tween 20
PEG	poly(ethylene glycol)
pFN	plasma fibronectin
PLL	poly-L-lysine

PMSF	phenylmethanesulfonyl fluoride
QCM-D	quartz crystal microbalance with dissipation
REF	rat embryonic fibroblast
ROI	region of interest
SDS-PAGE	sodium dodecyl sulfate-polyacrylamide gel electrophoresis
sFN	superfibronectin
TIRF	total internal reflection fluorescence
YFP	yellow fluorescent protein
YPet	a derivative of YFP: YFP for energy transfer

9 Acknowledgements

Finishing this project makes me think not only about the effort it took, but also about the help and support I received from so many people who made it possible for me to get here.
After finishing my Diploma thesis, I decided to stay in the Spatz Group to do my PhD. I was impressed by the working atmosphere, the motivating supervision by Ada Cavalcanti-Adam and the excellent equipment available in the group. I would like to thank Prof. Joachim Spatz for offering me the opportunity to do my dissertation in his group and for his motivating support. Essential for finishing the thesis was, of course, Ada, who was always there when I needed discussion, motivation and guidance.
It was very helpful to have the chance to give presentations about the progress of my project, not only within the Spatz Group, but also to my thesis advisory committee. I would like to specially thank Dr. Suat Özbek for both taking part in the yearly meetings as well as for being my first referee providing me with constructive criticism and a review of this thesis.
I would like to thank all my colleagues in the Spatz Group for the shared cake and coffee breaks and barbecues. Most of all I thank my office mates throughout this time for creating a fun working time. Special thanks to Rebecca Medda, Katharina Klein and Nadine Perschmann, who carefully read the draft of my dissertation. I thank Katharina, Nadine, Theresa, Vera and Silke for showing me how to use some of the equipment I used and Rebecca, Katharina and Claudio Rolli for their very appreciated help with Latex. I sincerely thank Tamás Haraszti for helpful discussions and for developing the macro used to analyze microscopy images. I am grateful to Christine Mollenhauer for the isolation and purification of FN, Sigrid Riese and Ling Cheng for their support in my experimental work.
I thank the people from the graduate school HBIGS who organized interesting courses, seminars and lectures, specially Rolf Lutz and Sandra Martini.
I would like to thank the following people for material support: Prof. Benny Geiger from the Weizmann Institute for Science in Israel for providing REF cells and showing interest in my work, Dr. David Staunton from the University of Oxford for sending the $FNIII_{9-10}$ fragment, Prof. Harold P. Erick-

son from the Duke University for providing MEFYpetFN cells and finally Prof. Reinhard Fässler and Josephine Gibson for providing MEF $FN^{fl/fl}$ and MEF $FN^{-/-}$ cells.
It would have also been nearly impossible for me to study in Heidelberg without the support from the German Academic Exchange Service. Through the DAAD I met students with whom I have lasting friendships, and specially close to me are Renate, Zuzi, Dani, Paula and Santo.
I would have probably never come to Germany if it hadn't been for Rolf Maier. He encouraged me to make my Deutsches Abitur, and together with his family made me feel a bit less far away from home, specially during my first months in Germany.
Last but not least, I thank all my friends in Germany and in Argentina for being so supportive and motivating with me. Very special thanks to Bart, who accompanied and encouraged me, specially during this last and very stressful year. Dankjewel, schatje! And of course, I thank my parents, my sister and my uncle for the sacrifice it meant to send me to a private German school, specially when our country started going through such difficult times.

References

[Akiyama et al., 1990] Akiyama, S. K., Nagata, K., and Yamada, K. M. (1990). Cell surface receptors for extracellular matrix components. *Biochim. Biophys. Acta*, 1031(1):91–110.

[Al-Jawad et al., 2009] Al-Jawad, M., Fragneto, G., Liu, J., Chang, S. R., and Clarkson, B. (2009). Fibronectin adsorption studied using neutron reflectometry and complementary techniques. *Eur Phys J E Soft Matter*, 30(2):175–9.

[Alberts et al., 2002] Alberts, B., Johnson, A., Lewis, J., Raff, M., Roberts, K., and Walter, P. (2002). *Molecular Biology of the Cell*. Garland Science, 4th edition.

[Allen and Jones, 2011] Allen, M. and Jones, J. L. (2011). Jekyll and Hyde: the role of the microenvironment on the progression of cancer. *J. Pathol.*, 223(2):162–76.

[Aota et al., 1994] Aota, S., Nomizu, M., and Yamada, K. M. (1994). The short amino acid sequence Pro-His-Ser-Arg-Asn in human fibronectin enhances cell-adhesive function. *J. Biol. Chem.*, 269(40):24756–61.

[Arnold et al., 2004] Arnold, M., Cavalcanti-Adam, E. A., Glass, R., Blümmel, J., Eck, W., Kantlehner, M., Kessler, H., and Spatz, J. P. (2004). Activation of integrin function by nanopatterned adhesive interfaces. *Chemphyschem*, 5(3):383–8.

[Asaga et al., 1991] Asaga, H., Kikuchi, S., and Yoshizato, K. (1991). Collagen gel contraction by fibroblasts requires cellular fibronectin but not plasma fibronectin. *Exp. Cell. Res.*, 193(1):167–74.

[Baneyx et al., 2002] Baneyx, G., Baugh, L., and Vogel, V. (2002). Fibronectin extension and unfolding within cell matrix fibrils controlled by cytoskeletal tension. *PNAS*, 99(8):5139–43.

[Bershadsky et al., 2003] Bershadsky, A. D., Balaban, N. Q., and Geiger, B. (2003). Adhesion-dependent cell mechanosensitivity. *Annu. Rev. Cell Dev. Biol.*, 19:677–95.

[Blümmel et al., 2007] Blümmel, J., Perschmann, N., Aydin, D., Drinjakovic, J., Surrey, T., Lopez-Garcia, M., Kessler, H., and Spatz, J. P. (2007). Protein repellent properties of covalently attached peg coatings on nanostructured sio(2)-based interfaces. *Biomaterials*, 28(32):4739–47.

[Brown and Discher, 2009] Brown, A. E. X. and Discher, D. E. (2009). Conformational changes and signaling in cell and matrix physics. *Curr. Biol.*, 19(17):R781–9.

[Brunner et al., 2011] Brunner, M., Millon-Frémillon, A., Chevalier, G., Nakchbandi, I. A., Mosher, D., Block, M. R., Albigès-Rizo, C., and Bouvard, D. (2011). Osteoblast mineralization requires β_1 integrin/ICAP-1-dependent fibronectin deposition. *J. Cell Biol.*, 194(2):307–22.

[Calderwood, 2004] Calderwood, D. A. (2004). Integrin activation. *J. Cell. Sci.*, 117(Pt 5):657–66.

[Cantor et al., 2008] Cantor, J. M., Ginsberg, M. H., and Rose, D. M. (2008). Integrin-associated proteins as potential therapeutic targets. *Immunol. Rev.*, 223:236–51.

[Cavalcanti-Adam, 2005] Cavalcanti-Adam, A. E. (2005). *The control of cell adhesion and adhesion-dependent events by nanotemplates regulating the spatial arrangement of integrin ligands.* PhD thesis, University of Heidelberg.

[Cavalcanti-Adam et al., 2007] Cavalcanti-Adam, E. A., Volberg, T., Micoulet, A., Kessler, H., Geiger, B., and Spatz, J. P. (2007). Cell spreading and focal adhesion dynamics are regulated by spacing of integrin ligands. *Biophysj*, 92(8):2964–74.

[Chauhan et al., 2005] Chauhan, A. K., Moretti, F. A., Iaconcig, A., Baralle, F. E., and Muro, A. F. (2005). Impaired motor coordination in mice lacking the EDA exon of the fibronectin gene. *Behav. Brain. Res.*, 161(1):31–8.

[Clark et al., 1986] Clark, R. A., Folkvord, J. M., and Nielsen, L. D. (1986). Either exogenous or endogenous fibronectin can promote adherence of human endothelial cells. *J. Cell Sci.*, 82:263–80.

[Cluzel et al., 2005] Cluzel, C., Saltel, F., Lussi, J., Paulhe, F., Imhof, B. A., and Wehrle-Haller, B. (2005). The mechanisms and dynamics of $\alpha_v\beta_3$ integrin clustering in living cells. *J. Cell Biol.*, 171(2):383–92.

[Fässler et al., 1995] Fässler, R., Martin, K., Forsberg, E., Litzenburger, T., and Iglesias, A. (1995). Knockout mice: how to make them and why. The immunological approach. *Int. Arch. Allergy Immunol.*, 106(4):323–34.

[Franza et al., 1986] Franza, B. R., Maruyama, K., Garrels, J. I., and Ruley, H. E. (1986). *In vitro* establishment is not a sufficient prerequisite for transformation by activated ras oncogenes. *Cell*, 44(3):409–18.

[Geiger and Yamada, 2011] Geiger, B. and Yamada, K. M. (2011). Molecular architecture and function of matrix adhesions. *Cold Spring Harb. Perspect. Biol.*, 3(5).

[George et al., 1993] George, E. L., Georges-Labouesse, E. N., Patel-King, R. S., Rayburn, H., and Hynes, R. O. (1993). Defects in mesoderm, neural tube and vascular development in mouse embryos lacking fibronectin. *Development*, 119(4):1079–91.

[Gonzalez and Wintz, 1987] Gonzalez, R. and Wintz, P. (1987). Digital image processing. *Addison-Wesley Educational Publishers Inc (December 1978)*.

[Grant et al., 1997] Grant, R. P., Spitzfaden, C., Altroff, H., Campbell, I. D., and Mardon, H. J. (1997). Structural requirements for biological activity of the ninth and tenth FIII domains of human fibronectin. *J. Biol. Chem.*, 272(10):6159–66.

[Guadamillas et al., 2011] Guadamillas, M. C., Cerezo, A., and Pozo, M. A. D. (2011). Overcoming anoikis - pathways to anchorage-independent growth in cancer. *J. Cell. Sci.*, 124(Pt 19):3189–97.

[Guan et al., 1990] Guan, J. L., Trevithick, J. E., and Hynes, R. O. (1990). Retroviral expression of alternatively spliced forms of rat fibronectin. *J. Cell Biol.*, 110(3):833–47.

[Harburger and Calderwood, 2009] Harburger, D. S. and Calderwood, D. A. (2009). Integrin signalling at a glance. *J. Cell. Sci.*, 122(Pt 2):159–63.

[Hino et al., 1996] Hino, K., Maeda, T., Sekiguchi, K., Shiozawa, K., Hirano, H., Sakashita, E., and Shiozawa, S. (1996). Adherence of synovial cells on EDA-containing fibronectin. *Arthritis Rheum.*, 39(10):1685–92.

[Humphries et al., 2006] Humphries, J. D., Byron, A., and Humphries, M. J. (2006). Integrin ligands at a glance. *J. Cell. Sci.*, 119(Pt 19):3901–3.

[Humphries et al., 2007] Humphries, J. D., Wang, P., Streuli, C., Geiger, B., Humphries, M. J., and Ballestrem, C. (2007). Vinculin controls focal adhesion formation by direct interactions with talin and actin. *J. Cell Biol.*, 179(5):1043–57.

[Huveneers et al., 2008] Huveneers, S., Truong, H., Fässler, R., Sonnenberg, A., and Danen, E. H. J. (2008). Binding of soluble fibronectin to integrin α_5 β_1 - link to focal adhesion redistribution and contractile shape. *J. Cell Sci.*, 121(Pt 15):2452–62.

[Hynes, 2002] Hynes, R. O. (2002). Integrins: bidirectional, allosteric signaling machines. *Cell*, 110(6):673–87.

[Ingham et al., 1997] Ingham, K. C., Brew, S. A., Huff, S., and Litvinovich, S. V. (1997). Cryptic self-association sites in type III modules of fibronectin. *J. Biol. Chem.*, 272(3):1718–24.

[Johnson et al., 1999] Johnson, K. J., Sage, H., Briscoe, G., and Erickson, H. P. (1999). The compact conformation of fibronectin is determined by intramolecular ionic interactions. *J. Biol. Chem.*, 274(22):15473–9.

[Kadler et al., 2008] Kadler, K. E., Hill, A., and Canty-Laird, E. G. (2008). Collagen fibrillogenesis: fibronectin, integrins, and minor collagens as organizers and nucleators. *Curr. Opin. Cell Biol.*, 20(5):495–501.

[Kalluri and Zeisberg, 2006] Kalluri, R. and Zeisberg, M. (2006). Fibroblasts in cancer. *Nat. Rev. Cancer*, 6(5):392–401.

[Kanters et al., 2001] Kanters, S. D., Banga, J. D., Algra, A., Frijns, R. C., Beutler, J. J., and Fijnheer, R. (2001). Plasma levels of cellular fibronectin in diabetes. *Diabetes Care*, 24(2):323–7.

[Katz et al., 2000] Katz, B. Z., Zamir, E., Bershadsky, A., Kam, Z., Yamada, K. M., and Geiger, B. (2000). Physical state of the extracellular matrix regulates the structure and molecular composition of cell-matrix adhesions. *Mol. Biol. Cell*, 11(3):1047–60.

[Klotzsch et al., 2009] Klotzsch, E., Smith, M. L., Kubow, K. E., Muntwyler, S., Little, W. C., Beyeler, F., Gourdon, D., Nelson, B. J., and Vogel, V. (2009). Fibronectin forms the most extensible biological fibers displaying switchable force-exposed cryptic binding sites. *PNAS*, 106(43):18267–72.

[Knecht et al., 2009] Knecht, S., Ricklin, D., Eberle, A. N., and Ernst, B. (2009). Oligohis-tags: mechanisms of binding to Ni^{2+}-NTA surfaces. *J. Mol. Recognit.*, 22(4):270–9.

[Kohan et al., 2010] Kohan, M., Muro, A. F., White, E. S., and Berkman, N. (2010). EDA-containing cellular fibronectin induces fibroblast differentiation through binding to $\alpha_4\beta_7$ integrin receptor and MAPK/erk 1/2-dependent signaling. *FASEB J.*, page (published ahead of print).

[Kornblihtt et al., 1996] Kornblihtt, A. R., Pesce, C. G., Alonso, C. R., Cramer, P., Srebrow, A., Werbajh, S., and Muro, A. F. (1996). The fibronectin gene as a model for splicing and transcription studies. *FASEB J.*, 10(2):248–57.

[Kornblihtt et al., 1985] Kornblihtt, A. R., Umezawa, K., Vibe-Pedersen, K., and Baralle, F. E. (1985). Primary structure of human fibronectin: differential splicing may generate at least 10 polypeptides from a single gene. *EMBO J.*, 4(7):1755–9.

[Lemmon et al., 2009] Lemmon, C. A., Chen, C. S., and Romer, L. H. (2009). Cell traction forces direct fibronectin matrix assembly. *Biophys. J.*, 96(2):729–38.

[Li et al., 2004] Li, Q., Lau, A., Morris, T. J., Guo, L., Fordyce, C. B., and Stanley, E. F. (2004). A syntaxin 1, Gα(o), and N-type calcium channel complex at a presynaptic nerve terminal: analysis by quantitative immunocolocalization. *J. Neurosci.*, 24(16):4070–81.

[Liao et al., 2002] Liao, Y.-F., Gotwals, P. J., Koteliansky, V. E., Sheppard, D., and Water, L. V. D. (2002). The EIIIA segment of fibronectin is a ligand for integrins $\alpha_9\beta_1$ and $\alpha_4\beta_1$ providing a novel mechanism for regulating cell adhesion by alternative splicing. *J. Biol. Chem.*, 277(17):14467–74.

[Lodish et al., 2000] Lodish, H., Berk, A., Zipursky, S. L., Matsudaira, P., Baltimore, D., and Darnell, J. (2000). *Molecular Cell Biology*. W. H. Freeman, 4th edition.

[Lohmüller et al., 2011] Lohmüller, T., Aydin, D., Schwieder, M., Morhard, C., Louban, I., Pacholski, C., and Spatz, J. P. (2011). Nanopatterning by block copolymer micelle nanolithography and bioinspired applications. *Biointerphases*, 6(1):MR1–12.

[Manabe et al., 1997] Manabe, R., Ohe, N., Maeda, T., Fukuda, T., and Sekiguchi, K. (1997). Modulation of cell-adhesive activity of fibronectin by the alternatively spliced EDA segment. *J. Cell Biol.*, 139(1):295–307.

[Manders and Verbeek, 1993] Manders, E. and Verbeek, F. (1993). Measurement of co-localization of objects in dual-colour confocal images. *J. Microsc.*

[Mao and Schwarzbauer, 2005a] Mao, Y. and Schwarzbauer, J. E. (2005a). Fibronectin fibrillogenesis, a cell-mediated matrix assembly process. *Matrix Biol.*, 24(6):389–99.

[Mao and Schwarzbauer, 2005b] Mao, Y. and Schwarzbauer, J. E. (2005b). Stimulatory effects of a three-dimensional microenvironment on cell-mediated fibronectin fibrillogenesis. *J. Cell Sci.*, 118(Pt 19):4427–36.

[Midwood et al., 2006] Midwood, K. S., Mao, Y., Hsia, H. C., Valenick, L. V., and Schwarzbauer, J. E. (2006). Modulation of cell-fibronectin matrix interactions during tissue repair. *J. Investig. Dermatol. Symp. Proc.*, 11(1):73–8. bajar pdf.

[Moretti et al., 2007] Moretti, F. A., Chauhan, A. K., Iaconcig, A., Porro, F., Baralle, F. E., and Muro, A. F. (2007). A major fraction of fibronectin present in the extracellular matrix of tissues is plasma-derived. *J. Biol. Chem.*, 282(38):28057–62.

[Ohashi and Erickson, 2009] Ohashi, T. and Erickson, H. P. (2009). Revisiting the mystery of fibronectin multimers: the fibronectin matrix is composed of fibronectin dimers cross-linked by non-covalent bonds. *Matrix Biol.*, 28(3):170–5.

[Pankov et al., 2000] Pankov, R., Cukierman, E., Katz, B. Z., Matsumoto, K., Lin, D. C., Lin, S., Hahn, C., and Yamada, K. M. (2000). Integrin dynamics and matrix assembly: tensin-dependent translocation of $\alpha_5\beta_1$ integrins promotes early fibronectin fibrillogenesis. *J. Cell Biol.*, 148(5):1075–90.

[Pereira et al., 2002] Pereira, M., Rybarczyk, B. J., Odrljin, T. M., Hocking, D. C., Sottile, J., and Simpson-Haidaris, P. J. (2002). The incorporation of fibrinogen into extracellular matrix is dependent on active assembly of a fibronectin matrix. *J. Cell Sci.*, 115(Pt 3):609–17.

[Sabatier et al., 2009] Sabatier, L., Chen, D., Fagotto-Kaufmann, C., Hubmacher, D., McKee, M. D., Annis, D. S., Mosher, D. F., and Reinhardt, D. P. (2009). Fibrillin assembly requires fibronectin. *Molecular Biology of the Cell*, 20(3):846–58.

[Sakai et al., 2001] Sakai, T., Johnson, K. J., Murozono, M., Sakai, K., Magnuson, M. A., Wieloch, T., Cronberg, T., Isshiki, A., Erickson, H. P., and Fässler, R. (2001). Plasma fibronectin supports neuronal survival and reduces brain injury following transient focal cerebral ischemia but is not essential for skin-wound healing and hemostasis. *Nat. Med.*, 7(3):324–30.

[Shattil et al., 2010] Shattil, S. J., Kim, C., and Ginsberg, M. H. (2010). The final steps of integrin activation: the end game. *Nat. Rev. Mol. Cell Biol.*, 11(4):288–300.

[Shinde et al., 2008] Shinde, A. V., Bystroff, C., Wang, C., Vogelezang, M. G., Vincent, P. A., Hynes, R. O., and Water, L. V. D. (2008). Identification of the peptide sequences within the EIIIA (EDA) segment of fibronectin that mediate integrin $\alpha_9\beta_1$-dependent cellular activities. *J. Biol. Chem.*, 283(5):2858–70.

[Staunton et al., 2009] Staunton, D., Millard, C. J., Aricescu, A. R., and Campbell, I. D. (2009). Preparation of recombinant fibronectin fragments for functional and structural studies. *Methods Mol. Biol.*, 522:73–99.

[Takagi, 2004] Takagi, J. (2004). Structural basis for ligand recognition by RGD (Arg-Gly-Asp)-dependent integrins. *Biochem. Soc. Trans. Trans*, 32:403–6.

[Takagi and Springer, 2002] Takagi, J. and Springer, T. A. (2002). Integrin activation and structural rearrangement. *Immunological Reviews*, 186:141–163.

[To and Midwood, 2011] To, W. S. and Midwood, K. S. (2011). Plasma and cellular fibronectin: distinct and independent functions during tissue repair. *Fibrogenesis Tissue Repair*, 4:21.

[Waddington et al., 2009] Waddington, R. J., Youde, S. J., Lee, C. P., and Sloan, A. J. (2009). Isolation of distinct progenitor stem cell populations from dental pulp. *Cells Tissues Organs*, 189(1-4):268–74.

[Werner et al., 2007] Werner, S., Krieg, T., and Smola, H. (2007). Keratinocyte-fibroblast interactions in wound healing. *J. Invest. Dermatol.*, 127(5):998–1008.

[Wierzbicka-Patynowski and Schwarzbauer, 2003] Wierzbicka-Patynowski, I. and Schwarzbauer, J. E. (2003). The ins and outs of fibronectin matrix assembly. *J. Cell. Sci.*, 116(Pt 16):3269–76.

[Yamada and Kennedy, 1979] Yamada, K. M. and Kennedy, D. W. (1979). Fibroblast cellular and plasma fibronectins are similar but not identical. *J. Cell Biol.*, 80(2):492–8.

[Yamada and Olden, 1978] Yamada, K. M. and Olden, K. (1978). Fibronectins–adhesive glycoproteins of cell surface and blood. *Nature*, 275(5677):179–84.

[Zaidel-Bar et al., 2004] Zaidel-Bar, R., Cohen, M., Addadi, L., and Geiger, B. (2004). Hierarchical assembly of cell-matrix adhesion complexes. *Biochem. Soc. Trans.*, 32(Pt3):416–20.

[Zamir and Geiger, 2001] Zamir, E. and Geiger, B. (2001). Molecular complexity and dynamics of cell-matrix adhesions. *J. Cell Sci.*, 114(Pt 20):3583–90.

[Zamir et al., 1999] Zamir, E., Katz, B. Z., Aota, S., Yamada, K. M., Geiger, B., and Kam, Z. (1999). Molecular diversity of cell-matrix adhesions. *J. Cell Sci.*, 112:1655–69.

[Zamir et al., 2000] Zamir, E., Katz, M., Posen, Y., Erez, N., Yamada, K. M., Katz, B. Z., Lin, S., Lin, D. C., Bershadsky, A., Kam, Z., and Geiger, B. (2000). Dynamics and segregation of cell-matrix adhesions in cultured fibroblasts. *Nat. Cell Biol.*, 2(4):191–6.

[Zand et al., 2003] Zand, L., Qiang, F., Roskelley, C. D., Leung, P. C. K., and Auersperg, N. (2003). Differential effects of cellular fibronectin and plasma fibronectin on ovarian cancer cell adhesion, migration, and invasion. *In vitro Cell Dev. Biol. Anim.*, 39(3-4):178–82.

[Zhong et al., 1998] Zhong, C., Chrzanowska-Wodnicka, M., Brown, J., Shaub, A., Belkin, A. M., and Burridge, K. (1998). Rho-mediated contractility exposes a cryptic site in fibronectin and induces fibronectin matrix assembly. *J. Cell Biol.*, 141(2):539–51.

[Zimmerman et al., 2002] Zimmerman, E., Geiger, B., and Addadi, L. (2002). Initial stages of cell-matrix adhesion can be mediated and modulated by cell-surface hyaluronan. *Biophys. J.*, 82(4):1848–57.